

ADEGBOYE, M.A., KARNIK, A. and FUNG, W.-K. 2021. Numerical study of pipeline leak detection for gas-liquid stratified flow. *Journal of natural gas science and engineering* [online], 94, article 104054. Available from: <https://doi.org/10.1016/j.jngse.2021.104054>

# Numerical study of pipeline leak detection for gas-liquid stratified flow.

ADEGBOYE, M.A., KARNIK, A. and FUNG, W.-K.

2021

# Numerical study of pipeline leak detection for gas-liquid stratified flow

Mutiu Adesina Adegboye<sup>a</sup>, Aditya Karnik <sup>a\*</sup>, Wai-Keung Fung<sup>a,b</sup>

<sup>a</sup>School of Engineering, Robert Gordon University, Aberdeen AB10 7GJ, UK

<sup>b</sup>Department of Applied Computing and Engineering, Cardiff School of Technologies, Cardiff Metropolitan University, Llandaff Campus, Western Avenue, Cardiff, CF5 2YB, UK

\*Corresponding author; Tel: +44 (0)1224 263335, E-mail address: a.karnik@rgu.ac.uk

## Abstract

Multiphase flows are of paramount importance in the oil and gas industry, considering that most petroleum industries produce and transport oil and gas simultaneously. However, systematic research on pipeline leakage conveying more than one phase at a time is lacking attention. In this work, a numerical method is proposed to investigate the effect of two-phase gas-liquid leak flow behaviour in a subsea natural gas pipeline. The results of the simulations have been validated against the latest experimental and numerical data reported in the literature, and a good agreement has been obtained. The effect of leak sizes, longitudinal leak locations, multiple leakages and axial leak positions on the pressure gradient, flow rate and volume fractions in the pipeline were systematically investigated. The results show that the flow field parameters provide pertinent indicators in pipeline leakage detection. In particular, the upstream pipeline pressure could serve as a critical indicator for detecting leakage even if the leak size is small. Whereas, the downstream flow rate is a dominant leakage indicator if the flow rate monitoring is

23 chosen for leak detection. The results also reveal that when two leaks with different sizes co-  
24 occur in a single pipe, detecting the small leak becomes difficult if its size is below 25% of the  
25 large leak size. However, in the event of a double leak with equal sizes, the leak closer to the  
26 pipe upstream is easier to detect.

27 **Keywords:** Loss prevention; Multiphase flow; Natural gas transportation; Numerical simulation;  
28 Pipeline leak detection.

29

## 30 **1. Introduction**

31 Pipelines are one of the primary tools in the oil and gas industry, which play a unique role in the  
32 process of gathering and delivering petroleum, hydrocarbon exploration and transportation (Sun  
33 *et al.*, 2019; Wang *et al.*, 2021). The use of pipelines has extended over time because it provides  
34 an effective system to increase energy supply and has been considered the safest and the most  
35 economical and efficient means of petroleum transportation (Muggleton *et al.*, 2020). For  
36 example, the average estimated deaths due to accidents per ton-mile of shipped petroleum  
37 products using trucks, ships and rails are respectively 87%, 4% and 2.7% more than those using  
38 pipelines (Cramer *et al.*, 2015; Adegboye *et al.*, 2019). However, a leak in pipeline remains a  
39 major concern for both safety and contamination in the environment (Li *et al.*, 2019a) in daily  
40 operation, and the likelihood of developing leaks increases with the ages and service time of the  
41 pipeline (Li *et al.*, 2018; Mohammed *et al.*, 2019). Different factors that are accountable for  
42 pipeline leakage include corrosion, defects during installation and erection work (Bolotina *et al.*,  
43 2018).

44 A leak in subsea pipelines creates a serious problem in maintaining safe, reliable, and effective  
45 offshore production facilities (Li *et al.*, 2019b). Unlike leak on surface or water transportation

46 pipeline, which are also of great concern. A leak in a subsea pipeline always puts the marine  
47 environment at risk. It also causes devastating disasters, resulting in assets damage,  
48 environmental pollution, human casualties, and corporate reputation loss (Ajao *et al.*, 2018).  
49 Besides the harmful effect of submarine pipeline leakage on the aquatic animals, subsea pipeline  
50 leak often causes oil spills into the sea region, making the detection and diagnosis difficult (Li *et*  
51 *al.*, 2019b). Thereby, it costs a significant amount of money and time to clean up the  
52 contaminated regions (Wei and Masuri, 2019).

53 Several safety regulations include the safety (PIPES) Act of 2006 and 2016 in the USA (Scott  
54 and Scott, 2019), the United States of energy policy and safety regulation (Scott, 2018), British  
55 Standard BS 8010 (Movley, 2005), among others have been established to ensure safe pipeline  
56 operations (Kazeem *et al.*, 2017; Ijaola *et al.*, 2020). Despite stricter regulations and maintenance  
57 practice imposed by different governments, several pipeline leakages are often reported  
58 worldwide (Dasgupta, 2016; Joling, 2017). The amounts of resources lost to these incidents are  
59 enormous (Wei and Masuri, 2019). To reduce the effects of accidental pipeline leakage, it is  
60 paramount to monitor pipelines for timely and accurate leak detection. The early leak detection  
61 will aid quick response to seize petroleum discharge and mitigate associated risks such as fire,  
62 explosion and system downtime, and thus will extend the petroleum transportation facilities  
63 lifetime.

## 64 **2. Related Works**

65 Several studies on pipeline leak detection methods have been proposed in the literature (Ben-  
66 Mansour *et al.*, 2012; Karim *et al.*, 2015; Wang and Ghidaoui, 2018; Syed *et al.*, 2020; Wang *et*  
67 *al.*, 2021). Existing leak detection and diagnostic are classified into software and hardware

68 approaches. In an effort to classify these technologies based on the technical nature, further  
69 research efforts were made and led to the classification into three groups, namely external, visual  
70 or biological and internal methods (Adegboye *et al.*, 2019). The external technologies utilise  
71 human-made sensing devices to achieve leak detection tasks at the exterior part of the pipeline.  
72 The visual-based methods employ experienced personnel, trained dogs, pigs and drones to  
73 inspect and detect pipeline leakage. This approach appears to be the most suitable for leak  
74 detection and localisation. However, the operational time of these techniques is based on the  
75 frequency of inspection. Readers are referred to Adegboye *et al.* (2019) for further details on the  
76 review of pipeline leakage detection methods.

77 Many researchers have reported a collection of techniques to detect and localise pipeline leakage  
78 for the internal-based leak detection methods. Generally, these methods employ computational  
79 algorithms in conjunction with various sensors for monitoring parameters that quantitatively  
80 characterise the fluid flow within pipelines. Some commonly used techniques include mass-  
81 volume balance (Karim *et al.*, 2015; Syed *et al.*, 2020), negative pressure wave (Elaoud *et al.*,  
82 2010; Datta and Sarkar, 2016; Chen *et al.*, 2018), pressure point analysis (bin Md *et al.*, 2011),  
83 state estimator (Ali *et al.*, 2015, Chen *et al.*, 2021), and dynamic modelling (Yang *et al.*, 2010; Li  
84 *et al.*, 2019b). Among these methods, dynamic modelling, also known as real-time transient  
85 modelling, is the most sensitive method (Guerriero *et al.*, 2016; Liu *et al.*, 2019). This method  
86 employs conservation equations for the fluid mass, momentum and energy to model the flow  
87 within a pipeline and compares the predicted values with the measured data to determine and  
88 characterise leakages. The flow parameters monitored in this method are flow rate, pressure, and  
89 other fluid flow parameters. Pipeline leak detection using transient-based leak detection approach  
90 has been extensively adopted in the research community (Araújo *et al.*, 2013; Araújo *et al.*,

91 2014; Lazhar *et al.*, 2013; De Sousa and Romero, 2017; Fu *et al.*, 2020; Ranawat and Nandwana,  
92 2021), and it has been shown to be successful in detecting and locating pipeline leak position.  
93 However, most of the work reported in the literature is limited to single-phase systems (Elaoud *et*  
94 *al.* 2010; Yang *et al.*, 2010; Lazhar *et al.*, 2013; Araújo *et al.* 2014; Ben-Mansour *et al.* 2012; De  
95 Sousa and Romero 2017; Li *et al.*, 2019; Wang *et al.*, 2021).

96 De Sousa and Romero (2017) investigated oil leak influence on the pressure and flow rate  
97 characteristics using ANSYS Fluent. The obtained results revealed how the leak impacted both  
98 pressure and flow rate within the leak region vicinity. Molina-Espinosa *et al.* (2013) carried out  
99 numerical modelling backed up by physical experiments for pipe leaks. In this study, transient  
100 modelling of incompressible flow in short pipes with leaks was investigated. The obtained results  
101 revealed good correlations between the simulation and experimental data in terms of pressure  
102 drop within the vicinity of the leakages.

103 A relevant study on subsea pipelines by Zhu *et al.* (2014) simulated oil released from submarine  
104 pipelines subjected to different leak sizes. In this study, the effects of oil leak rate, leak sizes, oil  
105 density and water velocity on the oil spill behaviour were investigated using the Volume of Fluid  
106 (VOF) method. This study revealed that small leak size, slow leaking and high fluid density led  
107 to a long period for oil to reach the maximum horizontal migrate distance. In a similar study by  
108 Li *et al.* (2018), a numerical investigation of submarine pipeline spillage was carried out using  
109 ANSYS Fluent to forecast oil spill trajectory movement. The quantity and trajectory of spilt oil  
110 under various operating pressure, current sea velocities and wavelengths were analysed.

111 Li *et al.* (2017) employed Computational Fluid Dynamics (CFD) models to describe underwater  
112 oil release rate and its trajectory movement from the damaged subsea pipeline to the free surface

113 of the water. The simulated results revealed that the developed model could provide a detailed  
114 understanding of pipeline leakage, such as gas release rate, horizontal dispersion distance and  
115 gas rising time in a subsea environment. However, gas movement trajectory behaviour can only  
116 be predicted in a shallow ocean as the sea wave can easily alter the leaking fluid dispersion  
117 movement. The approach to the subsea pipeline leakages reported in the literature (Zhu *et al.*,  
118 2014; Li *et al.*, 2017; Singh *et al.*, 2017) shows that consideration of the impact of leaks on fluid  
119 flow parameters within the pipeline in a subsea environment is yet to be well understood.

120 The extensive review reveals that literature on a multiphase pipeline leakage is rather limited.  
121 Most of the available literature focuses on single-phase flow. Multiphase flow systems are  
122 generally encountered not only in the oil and gas industry, nuclear, chemical process industries,  
123 among others. As such, the development of an accurate leak prediction model is timely and  
124 essential as this will aid in advancing rapid pipeline leak detection technologies for these critical  
125 applications.

126 In the context of multiphase pipeline leak detection, the computational study by Kam (2010)  
127 investigated the influence of leak sizes and the longitudinal locations of the leak on flow  
128 parameters. However, this study was only limited to a 1-D pipeline, assuming that the pipeline  
129 was made up of a series of small segments in which each node along the pipe modelled the local  
130 flow characteristics. A similar study presented by Figueiredo *et al.* (2017) investigated the effect  
131 of leakage on two-phase flow behaviour in nearly horizontal pipelines. In their study, the impact  
132 of longitudinal leak location on stratified flows was investigated. The finding revealed that  
133 pressure profiles commonly employed in monophasic leakage's could be extended to the stratified  
134 flow system. The limitation of this work, however, restriction to a 1-D pipeline. The empirical

135 models do not adequately capture all the dynamics of the multiphase flow behaviour. These  
136 analytical solution assumptions restrict their capability to consider different scenarios in which  
137 leak may occur in 3-D pipelines.

138 The 3-D CFD modelling approach promises to be an effective tool to investigate complex  
139 multiphase flow problems (Singh *et al.*, 2017; Saedipour *et al.*, 2019; Alghurabi *et al.*, 2021). It  
140 avoids unrealistic assumptions usually adopted in the empirical models for multiphase pipeline  
141 leakage. CFD models provide an opportunity to incorporate intricate pipeline configuration and  
142 offer detailed information of multiphase flow systems that may be difficult to obtain using  
143 analytical models or physical experiments. In particular, 3-D CFD models can readily investigate  
144 the influence of the radial position of the leak along the circumference of the pipe relative to the  
145 gas-liquid interface. Araújo *et al.* (2013) investigated leak influence in hydrodynamics of oil-  
146 water two-phase flow in a horizontal pipeline. The simulation was performed in ANSYS CFX  
147 using the Eulerian-Eulerian model by considering the oil as a continuous phase and water as a  
148 dispersed phase. The authors varied the volume fraction of oil at the inlet of the pipeline. They  
149 observed that the amount of oil discharged from the leak region reaches a stable value after  
150 around 0.4 s for all the simulations reported in their study. However, their study is limited to the  
151 leak effect before the flow stability time. Also, their study applicability may be limited since they  
152 did not report a particular flow pattern. Besides, the effects of radial and longitudinal leak  
153 locations, leak opening sizes and multiple leakages remain to be investigated. To better  
154 understand the fluid flow behaviour induced by leak for the aforementioned effects, the present  
155 study extends the multiphase pipeline leakage to both before and after the flow stability state.

156 This study motivation is the lack of research that systematically investigates pipeline leakage  
157 conveying more than one phase at a time. A number of studies have been carried out to  
158 understand monophasic pipeline leakages. However, not much is known regarding the multiphase  
159 pipeline system. A recent study by Behari *et al.* (2020) noted that the available leak detection  
160 techniques in the open literature fail to satisfactorily address multiphase pipeline leakage  
161 phenomena. There is no guarantee that the information available for single pipeline leak cases  
162 can be extended to multiphase pipeline system. This is evident that more insight into pipeline  
163 transporting more than one is needed to attain a thorough understanding of pipeline leakage in  
164 this context.

165 The present paper is primarily aimed at investigating accidental leakage of pipeline in a subsea  
166 environment as a multiphase flow system. Plausible leak scenarios which may occur in the field  
167 have been covered. A comprehensive assessment of different leak sizes, longitudinal leak  
168 locations, radial positions, and multiple leakages are performed for a gas-liquid pipeline using a  
169 3-D CFD model. Specifically, RANS equations are model to study pipeline leakage. The  
170 perturbation of the pertinent flow field indicators for different leak scenarios is reported, which is  
171 expected to help in improving the understanding of multiphase flow behaviour induced by leaks.  
172 The simulation results are validated against the numerical simulation by Chinello *et al.* (2019)  
173 and experimental data reported in Espedal (1998). In particular, monophasic and stratified flow  
174 behaviours induced by leaks are compared and validated with the experimental data reported by  
175 Monina-Espinosa *et al.* (2013). This study will lead to developing an improved multiphase  
176 pipeline leak prediction system, providing guides for timely detection of multiphase pipeline  
177 leakage, and preventing injuries and damage to properties.

178 The rest of the paper is organised as follows: Section 3 presents the computational model used  
 179 for analysis, while Section 4 gives details of the numerical method and parameters. Detailed  
 180 simulation results will be analysed and discussed in Section 5. The summary and conclusion of  
 181 the research findings, including the recommendations for further work, are presented in Section  
 182 6.

183

### 184 **3. Computational model**

185 In order to describe multiphase flow modelling, it is required to solve the flow governing  
 186 equations together with the turbulence model. In this context, the flow governing equations and  
 187 turbulence model for air-water simulation are presented in this section.

188

#### 189 **3.1. Governing equations**

190 The VOF method and  $k - \omega$  SST turbulence models are applied for modelling stratified gas-  
 191 liquid flow in the pipeline. The flow is assumed to be incompressible, isothermal and adiabatic.  
 192 The VOF method, which is a one-fluid approach, comprises the continuity and momentum  
 193 equations which are given in Equations (1) and (2), respectively (Chinello *et al.*, 2019):

$$\frac{\partial \rho}{\partial t} + \nabla \cdot (\rho \vec{v}) = 0 \quad (1)$$

$$\frac{\partial}{\partial t} (\rho \vec{v}) + \nabla \cdot (\rho \vec{v} \vec{v}) = -\nabla p + \nabla \cdot (\bar{\tau} + \bar{\tau}_t) + \rho \vec{g} + \vec{F} \quad (2)$$

194 where  $\rho$  is the density of the mixing fluids,  $kg/m^3$ ;  $t$  is time,  $s$ ;  $\vec{v}$  is velocity vector after  
 195 Reynolds averaging,  $m/s$ ;  $p$  is static pressure,  $Pa$ ;  $\vec{g}$  is gravity force,  $m/s^2$ ;  $\vec{F}$  is a source term

196 accounting for the effect of surface tension. The molecular stress tensor  $\bar{\tau}$  is given as (Chinello *et*  
 197 *al.*, 2019; Li *et al.*, 2019a):

$$\bar{\tau} = \mu \left[ (\nabla \vec{v} + \nabla \vec{v}^T) - \frac{2}{3} \nabla \cdot \vec{v} I \right] \quad (3)$$

198 where  $\vec{v}^T$  is the transpose of the velocity vector, *m/s*. The turbulent stress tensor for the  
 199 Reynolds stress  $\bar{\tau}_t$  defined with the Boussinesq eddy viscosity approximation is defined as  
 200 (Chinello *et al.*, 2019):

$$\bar{\tau}_t = \mu_t \left[ (\nabla \vec{v} + \nabla \vec{v}^T) - \frac{2}{3} (\nabla \cdot \vec{v} + \rho k) I \right] \quad (4)$$

201 where  $I$  is unit tensor,  $\vec{v}^T$  is the transpose of the velocity vector, *m/s*. The surface tension force,  
 202  $\vec{F}$ , is modelled using the Continuum Surface Force (CSF) method due to Brackbill (1992).

203 The VOF model concept is applied to treat the two-phase gas-liquid as one single mixture in  
 204 accordance with the previous studies by Lo and Tomasello (2010) and Chinello *et al.* (2019).

205 The density ( $\rho$ ) and viscosity ( $\mu$ ) are volume fraction weighted mixture quantities:

$$\rho = \alpha_1 \rho_1 + \alpha_2 \rho_2 \quad (5)$$

$$\mu = \alpha_1 \mu_1 + \alpha_2 \mu_2 \quad (6)$$

206 where  $\alpha_1$  and  $\alpha_2$  are the volume fractions of the primary and secondary phases, respectively.

$$\alpha_1 + \alpha_2 = 1 \quad (7)$$

207 The volumetric transport equation for the secondary phase is determined using the following  
 208 equation:

$$\frac{\partial \alpha_2}{\partial t} + \vec{v} \cdot \nabla \alpha_2 = 0 \quad (8)$$

209 The pressure gradient is determined as:

$$\nabla p = dp/dx \quad (9)$$

210 where  $p$  is the pressure fields along the pipe;  $x$  is the position variable going along the length of  
 211 the pipe.

### 212 **3.2. Turbulence modelling**

213 Selection of an appropriate turbulence model is highly crucial in two-phase gas-liquid modelling  
 214 (Ali, 2017). Chinello *et al.* (2019) compared numerical simulations with the physical experiment  
 215 data conducted by Espedal (1998), which revealed that the  $k - \omega$  SST model yields better results  
 216 than both  $k - \omega$  and  $k - \varepsilon$  models for the air-water flow simulation if turbulence is properly  
 217 damped at the gas-liquid interface. Therefore, the  $k - \omega$  SST model is employed in this study,  
 218 and its constitutive equations are defined as follows:

219 The turbulence viscosity is given as (Chinello *et al.*, 2019):

$$\mu_t = \frac{\rho k}{\omega} \frac{1}{\max \left[ \frac{1}{\alpha^*}, \frac{SF_1}{a_1 \omega} \right]} \quad (10)$$

220 where  $k$  is turbulent kinetic energy, J/kg;  $\omega$  is specific dissipation rate,  $S$  is the strain rate  
 221 magnitude and is defined as:

$$S = \sqrt{2S_{ij}S_{ij}} \quad (11)$$

$$S_{ij} = \left( \frac{1}{2} \right) \left( \frac{\partial V_i}{\partial x_j} + \frac{\partial V_j}{\partial x_i} \right) \quad (12)$$

222 where  $S_{ij}$  is the average strain rate,  $V_i$  and  $V_j$  are the velocity components in  $x_i$  and  $x_j$  axis,  
 223 respectively. The transport equation for the turbulent kinetic energy;  $k$  and the specific  
 224 dissipation rate  $\omega$  is defined as:

$$\frac{D\rho k}{Dt} = \frac{\partial}{\partial x_j} \left[ \left( \mu + \frac{\mu_t}{\sigma_k} \right) \frac{\partial k}{\partial x_j} \right] + \min(\mu_t S^2, 10\rho\beta^* k\omega) - \rho\beta^* k\omega \quad (13)$$

$$\begin{aligned} \frac{D\rho\omega}{Dt} = & \frac{\partial}{\partial x_j} \left[ \left( \mu + \frac{\mu_t}{\sigma_\omega} \right) \frac{\partial \omega}{\partial x_j} \right] + \frac{\alpha}{V_t} \min(\mu_t S^2, 10\rho\beta^* k\omega) - \rho\beta\omega^2 + 2(1 - F_2)\rho \frac{1}{\sigma_\omega} \frac{\partial k}{2\omega} \frac{\partial \omega}{\partial x_j} \frac{\partial \omega}{\partial x_j} \\ & + S_\omega \end{aligned} \quad (14)$$

225 and the additional source term,  $S_\omega$ , is given as:

$$(S_\omega) = A\Delta n\beta\rho \left( \frac{B6\mu}{\beta\rho(\Delta n)^2} \right)^2 \quad (15)$$

226 where  $\Delta n$  is cell height normal to the interface,  $\beta$  is turbulence model constant and  $B$  is a  
 227 turbulence damping tuning parameter. The term  $A$  is the interface area density.

228 The blending functions  $F_1$  and  $F_2$  are defined as follows;

$$F_1 = \tanh \left[ \max \left( \frac{2\sqrt{k}}{0.09\omega y}, \frac{500\mu}{\rho y^2 \omega} \right) \right]^2 \quad (16)$$

$$F_2 = \tanh \left\{ \min \left[ \max \left( \frac{\sqrt{k}}{0.09\omega y}, \frac{500\mu}{\rho y^2 \omega} \right), \frac{4\rho k}{\sigma_{\omega,2} D_\omega^+ y^2} \right] \right\}^4 \quad (17)$$

229 where  $y$  is the distance to the closest wall surface,  $D_\omega^+$  is dimensionless specific dissipation rate.

230 The model constants are selected according to the  $k - \omega$  SST model of Chinello *et al.* (2019).

#### 231 4. Computational field

232 Fig. 1 presents the flow field domain of the proposed pipeline leak assessment modelling. The  
233 computational steps include mesh generation, boundary condition definitions, numerical method  
234 and code validation. For the results presented in this and subsequent sections, the pipeline inlet is  
235 treated as the reference location and all distances are measured relative to the pipeline inlet.

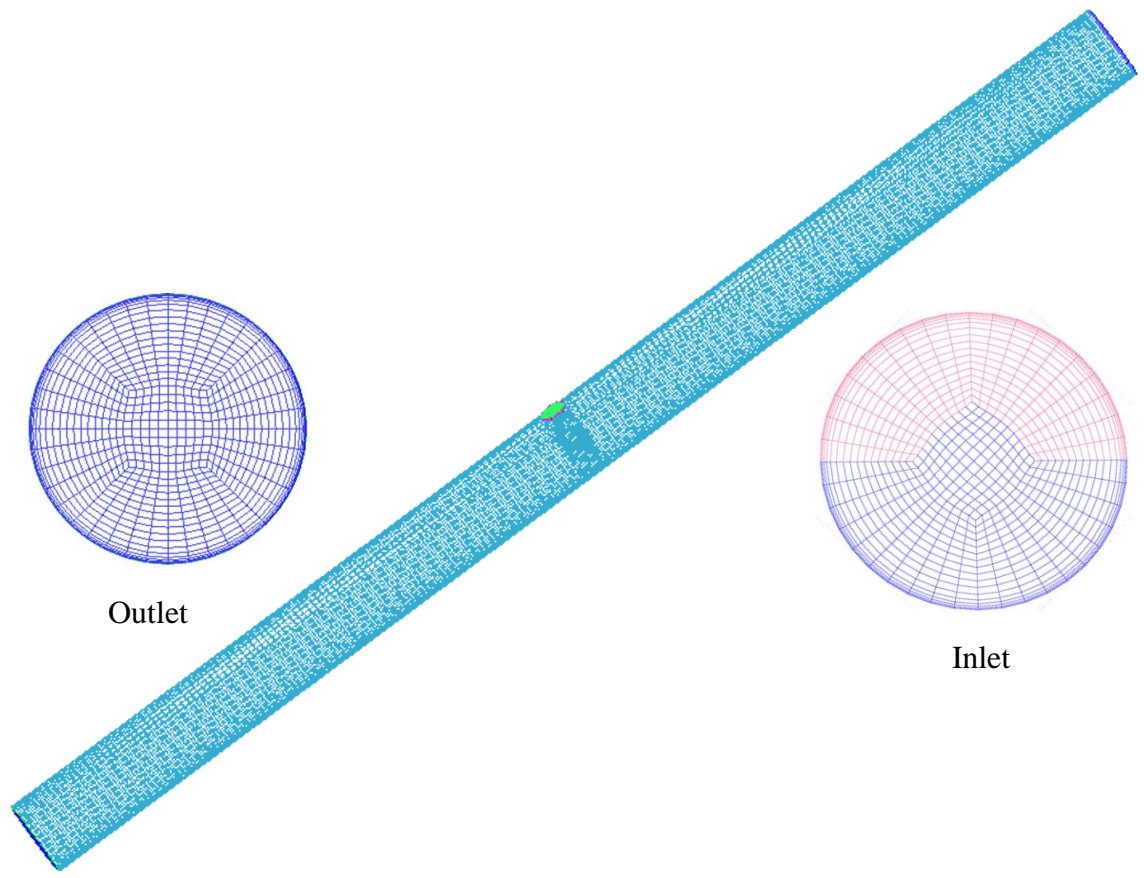
#### 236 **4.1. Mesh generation**

237 The numerical simulations are conducted on a 3-D horizontal pipeline with and without a leak. A  
238 pipe diameter of 0.06 m is employed in this study. The flow domain is divided into small discrete  
239 cells and meshed using structured mesh. This grid type allows the mesh refinement to be closer  
240 to the pipe wall and provides an opportunity to prevent singularities at the middle of the flow  
241 domain (Akhlaghi *et al.*, 2019). The mesh is generated such that the coarse mesh is in the centre,  
242 while the fine mesh is at the region near the pipe wall, as recommended by Akhlaghi *et al.*  
243 (2019). The mesh was developed using advanced functions, which resulted in its high quality  
244 with an average orthogonal quality of 0.99 (closer to 1.0) and skewness of 0.06. A grid  
245 dependence test was performed using various grid sizes to identify the most efficient grids for  
246 this study. In the grid independence study, superficial gas and liquid velocities were chosen as  
247 3.0 m/s and 0.32 m/s, respectively, which are similar to the numerical simulation values  
248 employed in Chinello *et al.* (2019) and physical experiment on stratified flow conducted by  
249 Espedal (1998).

250 The mesh independence analysis was performed by running simulation on grids with the smaller  
251 cells number. The grids size was further reduced, which subsequently led to the increases in  
252 grids number. Note that a mesh independent solution exists once changing in mesh size does not  
253 affect the final simulation. The grids sensitivity was performed by increasing the mesh sizes at

254 the cross-section of the pipe and along the pipe axis. Table 1 details the specifications of the  
255 employed grids, including its cross-sectional number and axial mesh cells. The mesh density  
256 effects are studied on the pressure drop characteristics. Fig. 2 (a) illustrates pressure drops at 1.5  
257 m away from the pipe upstream for the 3 m pipe with the 60 mm diameter. The figures show the  
258 pressure behaviours of mesh 1 to mesh 4 for the 20 s numerical simulation. The simulation  
259 results show that increases in grid numbers from mesh 2 to mesh 4 has little changes on the  
260 pressure drop, whereas the difference between mesh 1 and the other mesh sizes is massive. The  
261 pressure drop per unit length for the different mesh sizes at locations 1, 2 and 3 is shown in Fig.  
262 2(b). The figure indicates that the pressure drop does not change significantly between meshes 2,  
263 3 and 4. Therefore, mesh 2 was chosen for the numerical simulation as it demonstrates the  
264 optimum cells number for this study. Besides the simulation results' accuracy, simulation cost is  
265 essential to consider before one chosen mesh sizes for the simulation study. Therefore, mesh 2  
266 demonstrate the optimum mesh size for the present study as it satisfies both computational cost  
267 and accuracy.

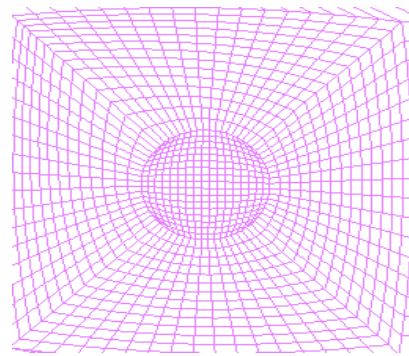
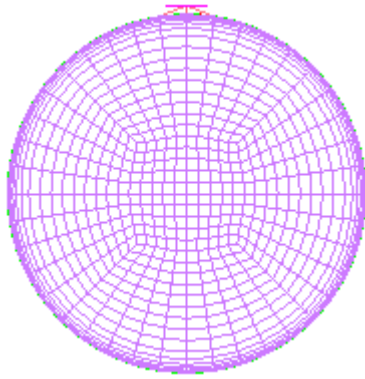
268



269

270

(a) Mesh generation for modelling pipeline leakage



271

272

(b) Cross-section view of the leakage

(c) Top view of the leakage

273

**Fig. 1.** Depiction of the mesh duct and detail of (a) Mesh generation for modelling pipeline

274

leakage, (b) Cross-section view of the leakage and (c) Top view of the leakage

275

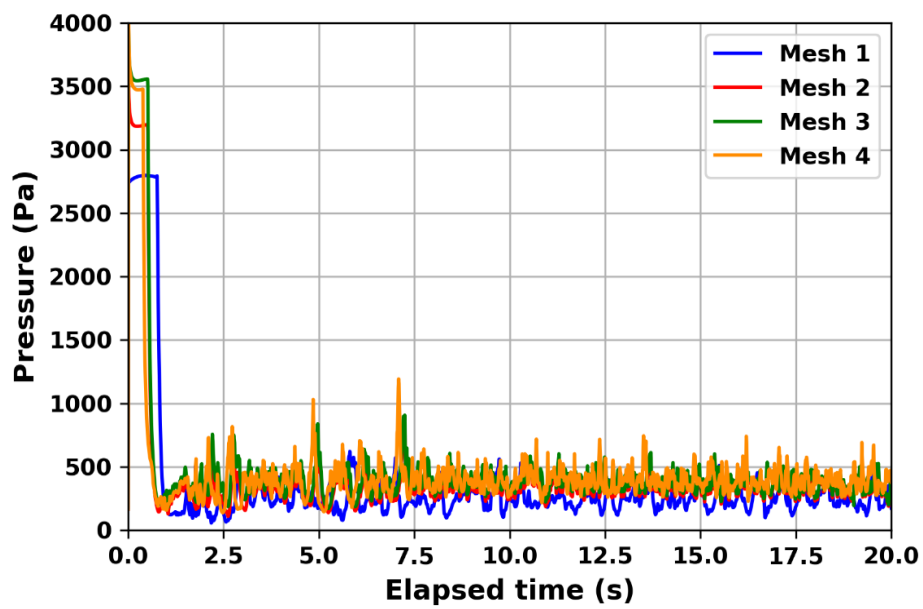
276

277

**Table 1:** Grids specification for mesh sensitivity analysis

Mesh name	Cross-sectional	Axial cells	Total
Mesh 1	511	400	204,400
Mesh 2	778	400	311,200
Mesh 3	1067	400	426,800
Mesh 4	1603	400	641,200

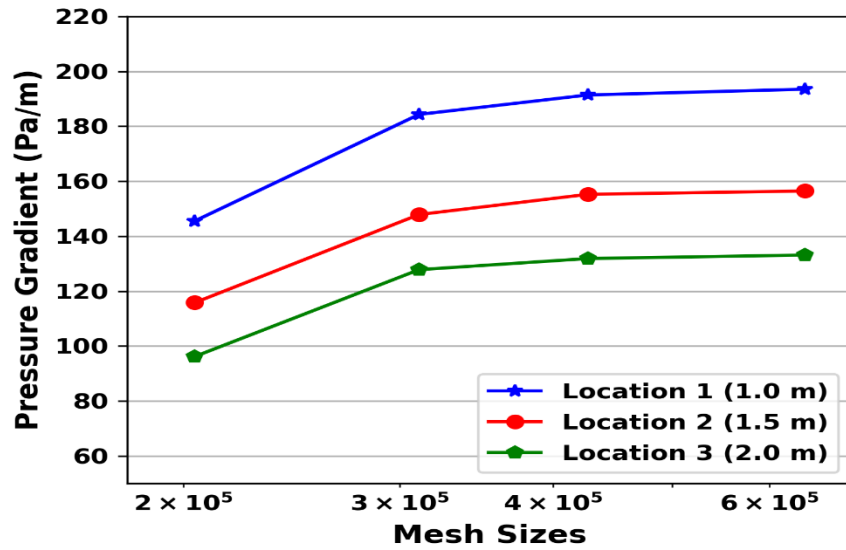
278



279

280

(a)



(b)

281

282

283 **Fig. 2:** Influence of variations in mesh density on model predictions: (a) mesh independency for  
 284 pressure drop at 1.5 m from the pipeline inlet, and (b) mesh size against pressure gradient across  
 285 selected locations along the pipe. Note that locations 1, 2 and 3 are set at 1.0 m, 1.5 m and 2.0 m,  
 286 respectively, away from the pipe upstream.

287

288 **4.2. Boundary conditions**

289 The pipeline inlet is set as a velocity inlet boundary defined by gas and liquid superficial  
 290 velocities. Injection of the two-phase into the computational domain can be done in two ways.  
 291 One method is to set the maximum velocity and non-slip volume fraction as boundary  
 292 conditions. After some distance, the separation between the mixed phases initiates along the  
 293 length of the pipe and distributes fluids into a specific pattern. In the second approach, which is  
 294 the method used in this study, the two phases are separately injected at the pipe inlet. One  
 295 significant advantage of this method is that flow can reach the fully developed condition sooner.  
 296 The gas is injected from the upper half cross-section of the pipe, while the liquid is injected from

297 the bottom half cross-section of the pipe. This resembles a separate flow structure, where each  
298 phase is separated into different layers, with the lighter fluid flowing on top of the denser fluid.  
299 The gas and liquid velocities at the inlet are specified to attain the target superficial velocities of  
300 the phases based on experimental data.

301 The physical properties of the fluid phases are presented in Table 2. The leak boundary is set as  
302 pressure outflow. The no-slip condition is applied at the pipe wall. Since the flow is assumed to  
303 be fully developed at the pipeline outlet, the backflow boundary pressure is imposed. The pipe is  
304 assumed to be in underwater condition, and the leak orifice and pipeline outlet pressures are  
305 defined constant, which is similar to that reported in Kam (2010) for pressure at 100 m below the  
306 sea surface (Wei and Masuri, 2019). In this instance, the pipeline outlet and leak surrounding  
307 pressures are scaled down to 400 Pa based on pipe diameter and simulation parameters in the  
308 present study.

309 **Table 2:** Fluid phases of physical properties

Property	Gas-phase	Liquid-phase
Density ( $\rho$ ), $\text{kg}/\text{m}^3$	1.225	998.2
Dynamic viscosity ( $\mu$ ), Pa.s	0.00001823	0.00091
Interfacial tension, N/m	0.0715	

310

### 311 **4.3. Numerical method**

312 The VOF modelling method is employed to simulate stratified gas-liquid flows. The computation  
313 is performed using a pressure-based solver, while the pressure fields are coupled with the  
314 velocity fields using SIMPLE pressure-velocity coupling scheme. The turbulence is modelled

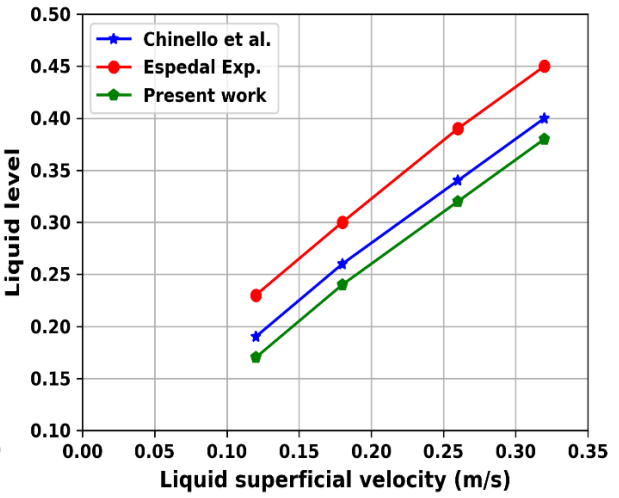
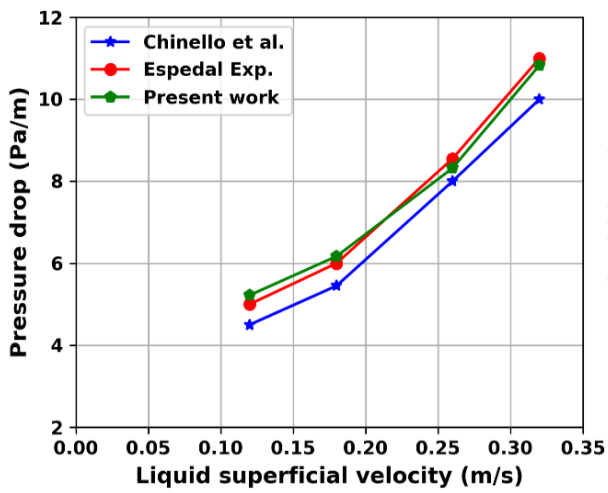
315 using the  $k - \omega$  SST model. The time-step used in the simulations is 0.001 s, and the simulated  
316 for 20, which is 20,000 iterations. All the computation run on an Intel(R) Xeon(R) Gold 6230  
317 CPU @ 2.10GHz, 16 Cores, 64.0 GB RAM. Please note that a single simulation required five  
318 days on average to complete on this computer. The momentum, turbulent kinetic energy and  
319 specific dissipation rate equations are discretised in space for the advection terms using a second-  
320 order upwind scheme in accordance with the study of Chinello *et al.* (2019). The discretisation of  
321 the volume fraction is performed using high-resolution interface capturing (HRIC) scheme  
322 (ANSYS, 2017). A first-order implicit temporal discretisation scheme is used to solve the  
323 governing equations. This method has been demonstrated to be reliable for evaluating pressure  
324 gradients and flow rates which are of interest in this work (Chinello *et al.*, 2019). The implicit  
325 algorithm is applied because the time derivative estimation can be obtained from neighbouring  
326 cells, which allows numerical calculation stable unconditionally with respect to the time-step  
327 size (Ali, 2017).

#### 328 ***4.4 Comparison with experimental data from the literature***

##### 329 ***4.4.1 Code validation***

330 The CFD code used in this study has been validated against the published experimental data in  
331 Espedal (1998) and numerical simulations reported in Chinello *et al.* (2019), which also  
332 employed the VOF model in ANSYS. Simulations are conducted using the VOF model for  
333 stratified air-water flow in a 3D pipe with the same experimental conditions as in these studies.  
334 The pipe used for the simulations is 18 m in length with a diameter of 0.06 m. The values of the  
335 model parameters for the density, interfacial tension and dynamic viscosity are given in Table  
336 2. The  $k - \omega$  SST turbulence model with the damping factor (B) of 250 is employed. Four sets of

337 numerical simulations were performed using the superficial gas velocity of 3 m/s, while the  
338 superficial liquid velocities were chosen as 0.12 m/s, 0.18 m/s, 0.26 m/s and 0.32 m/s. The  
339 pressure gradients are computed and compared against the experimental data. Fig. 3(a) shows the  
340 comparison of the present simulation results against the numerical simulations reported in  
341 Chinello *et al.* (2019), and experimental data reported in Espedal (1998). The obtained results  
342 demonstrate good agreement with the published CFD simulation results and experimental data.  
343 As shown in Fig. 3(a), the pressure gradient in the present simulation is more consistent with the  
344 experimental data than the simulation results reported in Chinello *et al.* The reason for the  
345 underestimation of liquid levels in Fig. 3(b) could be inherent from the liquid injection surface  
346 area of the pipe (see Fig. 1 for the inlet cross-section plane in boundary condition). Therefore, it  
347 should be admitted that there is a discrepancy in liquid levels obtained in both simulation and  
348 experiments due to the possible difference in the surface area of injection of the liquid phase.  
349 This validation has been undertaken to demonstrate the adequacy of the mesh and numerical  
350 schemes employed. In order to further ascertain the validity of our model, the predictive  
351 accuracy of the present simulations was tested against the experimental data of Strand (1993).  
352 Fig. 4 show comparisons of the pressure gradient between the current simulation and  
353 corresponding experiments data of Strand (1993). As shown in Fig. 4, the prediction matches the  
354 measurement data very well, with a deviation of less than 5%.



355

356

(a)

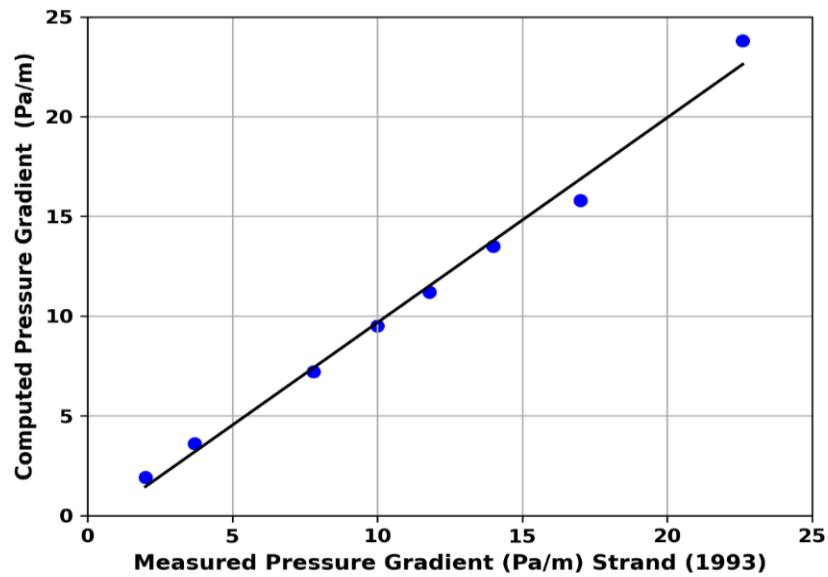
(b)

357 **Fig. 3.** Validation of numerical simulation model against experimental data reported in Espedal

358 *et al.* (1998) and numerical simulation results in Chinello *et al.* (2019); (a) pressure drop (Pa/m),

359

(b) Liquid level.



360

361 **Fig. 4.** Comparison of pressure gradient between current simulation and corresponding

362

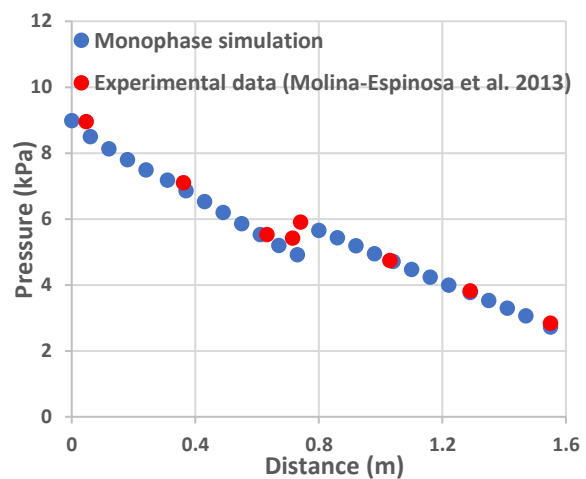
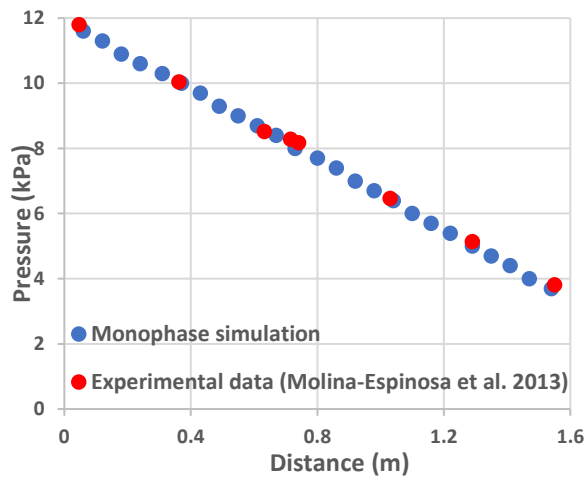
experiments data of Strand (1993)

#### 363 **4.4.2 Pipeline leaks comparison against experimental data**

364 Experimental data focused on the multiphase pipeline with the leak is seldomly reported and it is  
365 not easy to set up flow ring similar to the one reported in Molina-Espinosa et al. (2013), to test  
366 the gas-liquid, such as hydrocarbon and oil physical facility. The experimental data obtained  
367 from the same geometric model and simulation conditions in monophasic systems employed to  
368 verify that the boundary conditions. The pressure distribution proved effective and scientific to  
369 characterise stratified flow behaviours in this study. The effect of leak on stratified flow  
370 behaviours induced by leaks has previously been observed similar to the monophasic pipeline leakage  
371 in the previous study (Figueiredo et al. 2017). They concluded that the leak localisation strategy  
372 based on the upstream and downstream pressure profiles commonly employed in monophasic  
373 flow pipeline leakage could be extended to the stratified-flow system. However, all the data  
374 reported in that study was based on the 1-D pipeline.

375 The present stratified flow model carried out in a 3-D pipeline is compared with the monophasic  
376 flow system and validated with the experimental data reported by Molina-Espinosa *et al.* (2013).  
377 Molina-Espinosa *et al.* (2013) measured pressure distribution for the leak-free and leak diameters  
378 of 0.0033, 0.0052 and 0.0074 m, which form the leak sizes considered for the validation in the  
379 present study. The pipeline could be hundreds or thousands of meters long in reality; however,  
380 irrespective of the length of the pipeline, the pressure gradient would remain the same under  
381 normal flow condition. Therefore, a comparison between the simulation results obtained from the  
382 pipeline length considered in the present study and experimental data presented in (Molina-  
383 Espinosa et al. 2013) is scientifically sound.

384 The comparison of the pressure profile between experimental data and monophasic results is  
 385 shown in Fig. 5. The pressure profile without leak is illustrated in Fig. 5(a), and the resulting  
 386 pressure profile with leak sizes 0.0033, 0.0052 and 0.0074 m are shown in Fig. 5(b), Fig. 5(c),  
 387 and Fig. 5(d), respectively. Fig. 6 compares stratified flow against monophasic results in Fig. 5.  
 388 The monophasic and stratified flow models are set up based on the experimental configuration for  
 389 validation (Molina-Espinosa et al., 2013). As shown in Fig. 5, the monophasic simulation results  
 390 agree with the experimental data conducted on a single-phase scenario at a higher degree. The  
 391 pressure profile correlation in Fig. 6 reveals a slight divergence. The reason is that the stratified  
 392 model is made up of gas-liquid phases, leading to the gas release rate probably higher than the  
 393 liquid quantities under the same leak size. Statistical tests are applied to verify the consistency  
 394 among pressure data obtained from the monophasic simulation, stratified flow simulation and  
 395 experiments reported in Molina-Espinosa et al. (2013).

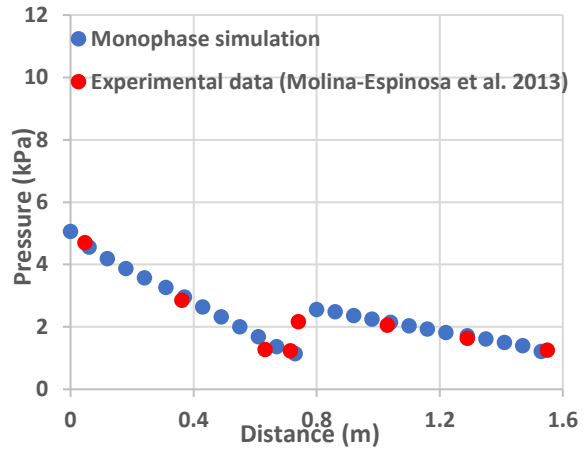
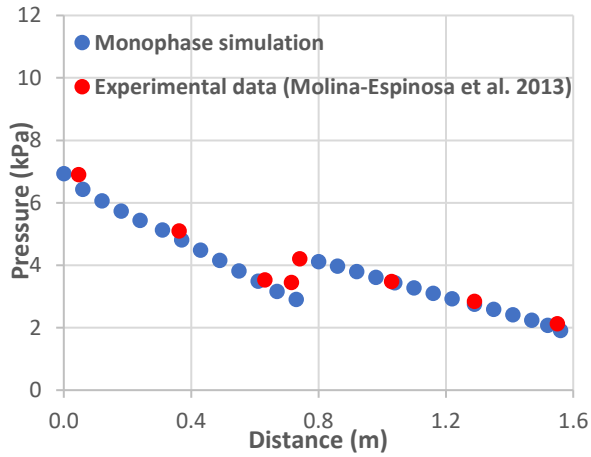


396

397

(a)

(b)



398

399

(c)

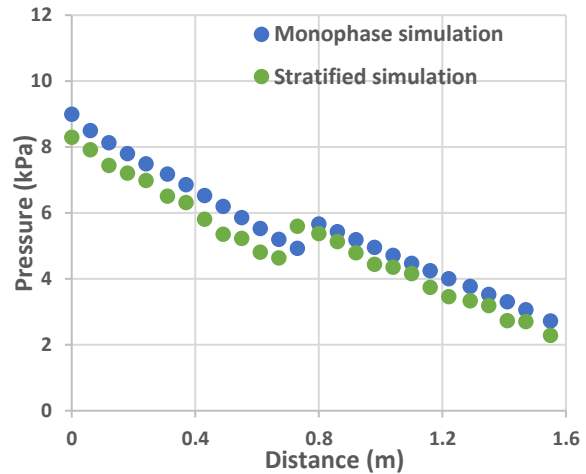
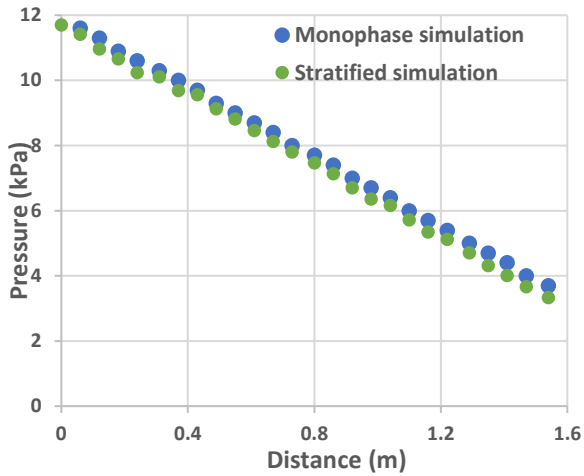
(d)

400

401

Fig. 5: Comparison for the pressure profile between the monophasic flow and the stratified flow model; (a) leak free, (b) 0.0033 m leak, (c) 0.0052 m leak, (d) 0.0074 m leak.

402

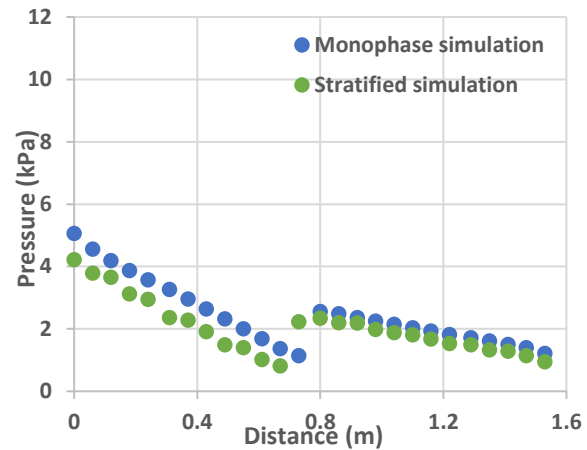
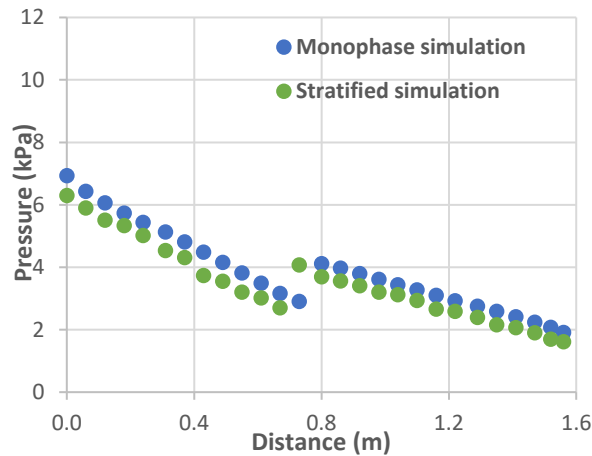


403

404

(a)

(b)



405

406

407 Fig. 6: Comparison for the pressure profile between the monophase flow and the stratified flow  
 408 model; (a) leak free, (b) 0.0033 m leak, (c) 0.0052 m leak, (d) 0.0074 m leak.

409

410 The statistical analysis was computed in MATLAB 2018b using one-way Analysis of Variance  
 411 (ANOVA) to compare the pressure gradient before and after the leak. The summary of the  
 412 hypothesis test results for the monophase simulations, experimental data and stratified model is  
 413 presented in Table 3. The p-values measure how much the means different of the three data  
 414 disagrees with the null hypothesis (the sample means of data taken from the 3 groups are equal).  
 415 As is clearly shown, the p-values for all the cases are range from 0.131 to 0.734, using 0.05  
 416 significance ( $\alpha$ ) level. These indicate that the mean difference between the three data are not  
 417 statistically significant and demonstrate strong evidence for the null hypothesis. We fail to reject  
 418 the null hypothesis at the significant level of 0.05.

419

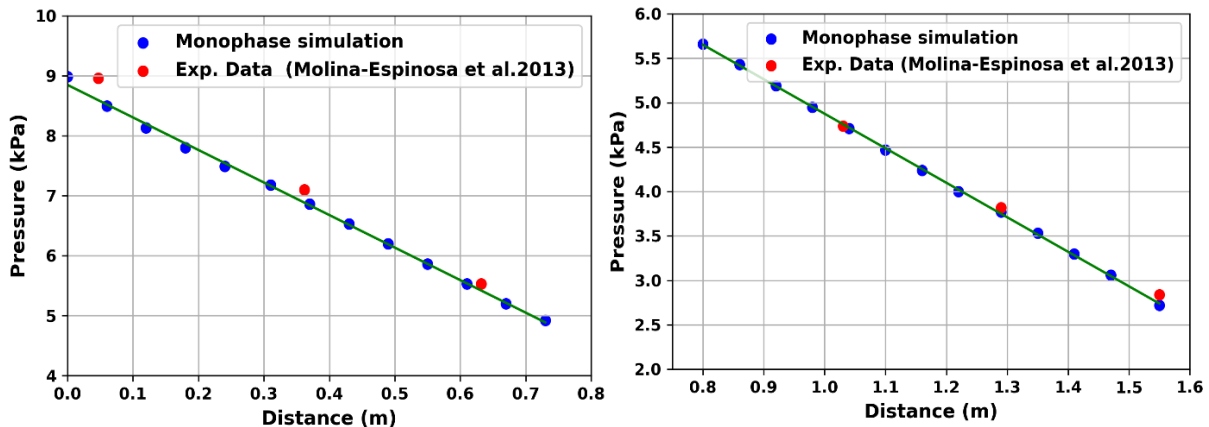
420

421

422 **Table 3:** Numerical (monophase and stratified) simulations and experimental data comparison  
 423 using one-way ANOVA; 0.05 significance ( $\alpha$ ) level

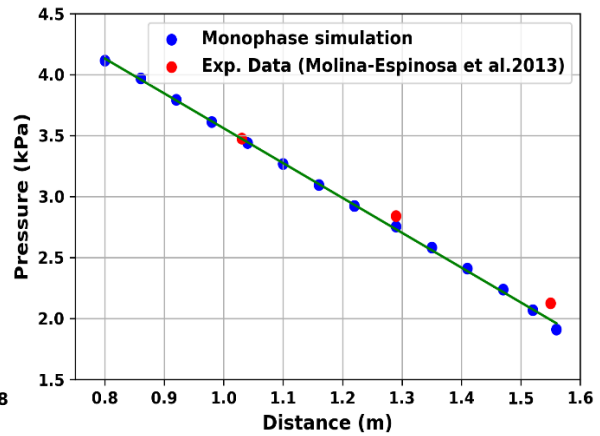
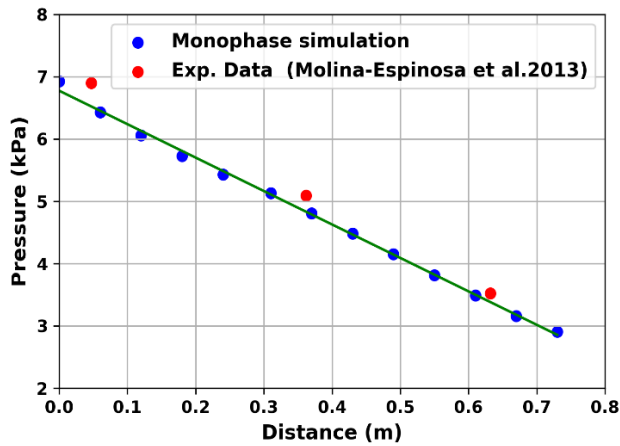
Leak scenario	Pressure gradient	p-values
Leak free	Upstream pressure	0.734
	Downstream pressure	0.747
Leak 1	Upstream pressure	0.382
	Downstream pressure	0.365
Leak 2	Upstream pressure	0.473
	Downstream pressure	0.354
Leak 3	Upstream pressure	0.365
	Downstream pressure	0.131

424  
 425 The linear regression plot shown in Fig. 7 demonstrates the adequate closeness of the  
 426 experimental and monophase simulation data points to the regression model. The average  
 427 variance of the experimental data from the fitness model is calculated using Mean Absolute  
 428 Deviation (MAD). The obtained results are presented in Table 4. From these results, the highest  
 429 MAD value is 0.263, which shows good agreement between the two data.

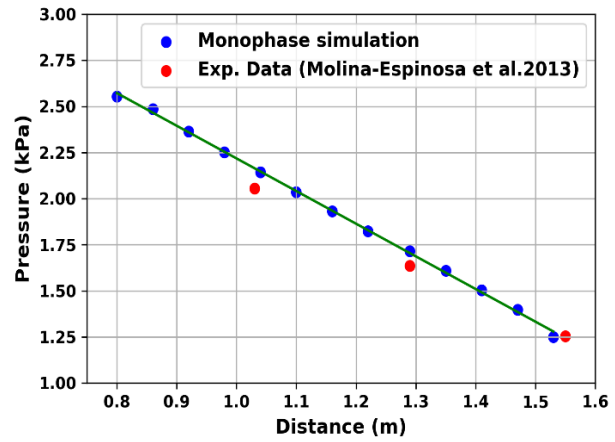
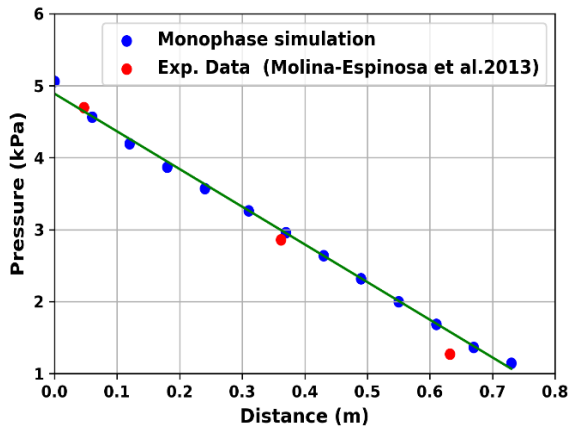


(a)leak 1

430  
 431



(b)Leak 2



(c)Leak 3

Fig. 7: Linear regression plot for monophase simulation against experimental data. Pressure gradient before leak (left) and pressure gradient after leak (right)

**Table 4:** The results of computed Mean Absolute Deviation (MAD) of experimental data from monophase simulation regression model.

Leak scenario	Pressure gradient	MAD
Leak free	Upstream pressure	0.060
	Downstream pressure	0.123
Leak 1	Upstream pressure	0.234
	Downstream pressure	0.060

Leak 2	Upstream pressure	0.263
	Downstream pressure	0.089
Leak 3	Upstream pressure	0.149
	Downstream pressure	0.061

---

441

442

443 Table 5 also presents the results of the hypothesis tests performed to determine whether the  
444 constants and coefficients of linear regression models of the monophasic and stratified pressure  
445 gradients variation before and after the leak are statistically significant. As demonstrated in the  
446 results shown in Table 5, the high R-square values indicate that the fitted linear regression  
447 models approximate the process which generates the data well. It is important to notice that the  
448 least R-squared value is 0.997 despite the multiphase coefficients p-value higher than 0.05. This  
449 indicates the possible disband among the stratified data due to the transient state of the  
450 multiphase model. These results agree to the previous study (Figueiredo et al. 2017) that  
451 concluded a leak localisation strategy based on the upstream and downstream pressure profiles  
452 commonly employed in monophasic flow pipeline leakage could be extended to the stratified-  
453 flow model. Therefore, the numerical models and simulation method used in this study have  
454 good quality and can well describe the fluids flow parameters distribution of pipeline leakage.  
455 Similarly, since multiphase flow system span beyond stratified flow pattern in order to have a  
456 better understanding of leak effect in all the multiphase system, comparison of other multiphase  
457 flow regimes such as bubble, slug, annular, etc. should be considered in future.

458

459 **Table 5:** Regression hypothesis results for monophasic and stratified simulations comparison

Leak scenario		R-Square	RSME	Constant p-value	Mono. Coef. p-value	Multiphase Coef. p-value
Leak free	Upstream pressure	0.998	0.033	$1.0295 \times 10^{-13}$	0.043353	0.28861
	Downstream pressure	<b>1.000</b>	0.005	$1.7711 \times 10^{-20}$	0.0005064	0.054394
Leak 1	Upstream pressure	0.998	0.011	$1.902 \times 10^{-12}$	0.0020	0.2820
	Downstream pressure	<b>1.000</b>	0.004	$4.4253 \times 10^{-20}$	$3.7577 \times 10^{-09}$	0.57519
Leak 2	Upstream pressure	0.998	0.009	$4.774 \times 10^{-13}$	0.0020	0.0690
	Downstream pressure	0.998	0.014	$7.8827 \times 10^{-19}$	$1.2721 \times 10^{-06}$	0.75957
Leak 3	Upstream pressure	0.998	0.012	$1.305 \times 10^{-11}$	0.0010	0.1890
	Downstream pressure	<b>0.997</b>	0.021	$3.1492 \times 10^{-14}$	0.0008683	0.84597

460

461

462 **5. Results and Discussions**

463 Numerical simulations are performed on a 3-D horizontal pipe with different leak scenarios.

464 Holes on pipe which are sources of leaks are assumed to be circular, and its distribution sizes are

465 determined based on International Association of Oil and Gas Producers (IOGP) recommended

466 hole sizes for subsea pipelines (Li *et al.*, 2018). According to the pipeline opening sizes

467 description specified in Li *et al.*, for a standard subsea pipeline with an average diameter of

468 0.334 m, a leak diameter of less than 0.02 m is regarded as a low leak. Moreover, a leak size

469 between 0.02 to 0.08 m is classified as medium leakage, while a leak diameter higher than 0.08

470 m is regarded as a large leak. The computed pipe opening dimensions for the 0.06 m diameter

471 pipe employed in this study follow the recommended values in IOGP and they are listed in Table

472 6. The superficial gas and liquid velocities used for pipeline leak modelling are 4.5 m/s and 0.5

473 m/s, respectively, while the pipeline length is 50 times the diameter. These values are determined  
 474 using the horizontal gas-liquid flow regime map so that stratified flow pattern is observed (Kanin  
 475 et al., 2019). The effect of leak sizes, longitudinal leak locations, axial leak positions and  
 476 multiple leakages are investigated, and results are presented for the flow rate, pressure gradient  
 477 and volume fractions in this section.

478 **Table 6:** Hole diameter used for the simulations

Hole size classes	Values (mm)	Leak size (percentage of pipe diameter)
Low	1.5	2.5%
Medium	9	15%
Large	14.5	24.2%
Rupture	18	30%

479

480 **5.1. Effect of leak magnitudes**

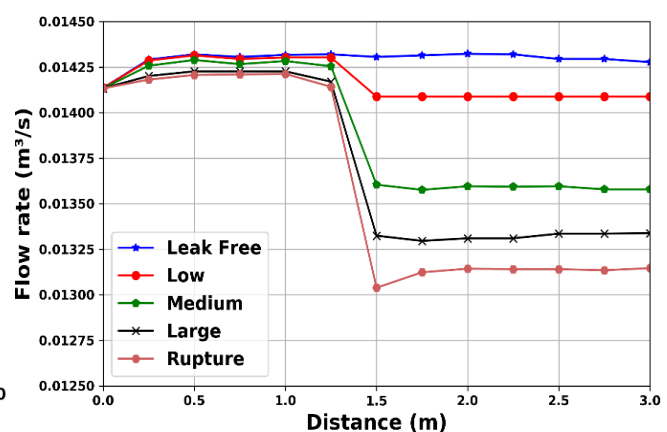
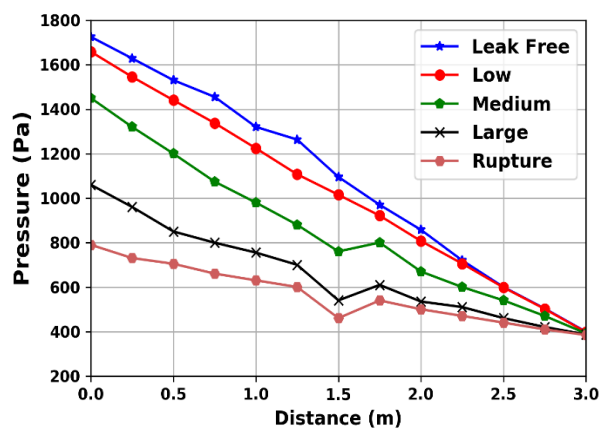
481 Leak size has a significant impact on the behaviour of fluids flow in the pipeline. In order to  
 482 study the effect of leak magnitude on the multiphase flow behaviour induced by the leak,  
 483 simulations of pipeline leakages for the different leak scenarios corresponding to the low,  
 484 medium, large and rupture scenarios are conducted and analysed. The leak is placed at the top-  
 485 middle part of the pipe, as shown in Fig. 1. Table 6 presents the values of the leak sizes  
 486 considered and its corresponding categories. The effects of leak size on the pressure gradient, the  
 487 flow rate and the volume fraction (gas void fraction and liquid holdup) at selected planes along

488 the pipeline are presented. The pressure response to the pipeline leak and how the response  
489 changes with leak sizes is shown in Fig. 8(a). As seen in Fig. 8(a), the pressure gradient remains  
490 identical under the leak-free scenario. The occurrence of leak leads to the reduction in pressure  
491 fields as the fluids try to escape through the leak. Although the existence of small leak leads to  
492 the decrease in pressure at the upstream of the pipe, the effect of the small leak is not significant  
493 at the leak location. This agrees with the analytical calculation in Kam (2010), which affirmed  
494 that the presence of a small leak is not visible at the location of the leakage. However, as the pipe  
495 leak opening size increases, more fluids tend to discharge through the orifice region. The similar  
496 pressure response can also be observed in physical experiment data reported in Molina-Espinosa  
497 *et al.* (2013) conducted on single-phase leakages.

498 As exemplified in Fig. 8(a), the magnitude of the pipeline opening size affects the rate of fluids  
499 discharge in the leak neighbourhood. The increase in fluids escaping from the leak medium leads  
500 to the rise in pressure drop, particularly within the vicinity of the leakage. This implies that the  
501 pressure profile around the neighbourhood of the leak can aid the accurate identification of leak  
502 location particularly when the leak is medium size or large. The presence of large leak size  
503 reveals that the larger the size of the leak, the more the fluids tend to discharge from the pipeline  
504 until it reaches the rupture stage. The effect of leak sizes on total flow rate characteristics based  
505 on various leak diameters is depicted in Fig. 8(b). It can be observed that the maximum decrease  
506 in flow rate suddenly occurs immediately after the leak position. There is no much significant  
507 variation in flow rate before the occurrence of leakage, but as the size of the leak increases, the  
508 fluids flow rate also reduces dramatically starting from the leak location. Therefore, the increases  
509 in pipe opening size result in the decrement of total flow rate downstream of the leak. This  
510 implies that flow rate decreases with increasing leak size. From the flow responses depicted in

511 Fig. 8, we conclude that upstream pressure serves as a pertinent indicator to detection of leakage  
 512 as it appears to be the most sensitive indicator even if the size of the leak is small. Whereas,  
 513 downstream flow rate response will be more favourable for leak detection if the flow transducer  
 514 is deployed downstream.

515 Fig. 9 presents the volume fraction contours at 2.5 m along the pipe under the same leak  
 516 scenarios shown in Fig. 8. The blue colour denotes the air void fraction, while the red indicates  
 517 the liquid holdup. As seen in Fig. 9(a), the air void fraction and the liquid holdup are distributed  
 518 equally in the absence of leakage. The occurrence of leak leads to the reduction in air void  
 519 fraction downstream of the pipe, which causes an increase in the liquid holdup. By comparing  
 520 the fluids volume fraction under different leak sizes shown in Fig. 8, it shows that leak size has a  
 521 significant influence on the saturation of fluids flow. Overall, the larger the leak size, the more  
 522 the relative amount of gas discharged from the pipeline if the leak is located at the top upper part  
 523 of the pipe. Therefore, the gas void fraction downstream of the leak becomes lower, which  
 524 eventually increases the liquid holdup. This occurs because the gas is less dense and more mobile  
 525 than liquid leading to the liquid replacing the escaped gas in the pipeline.



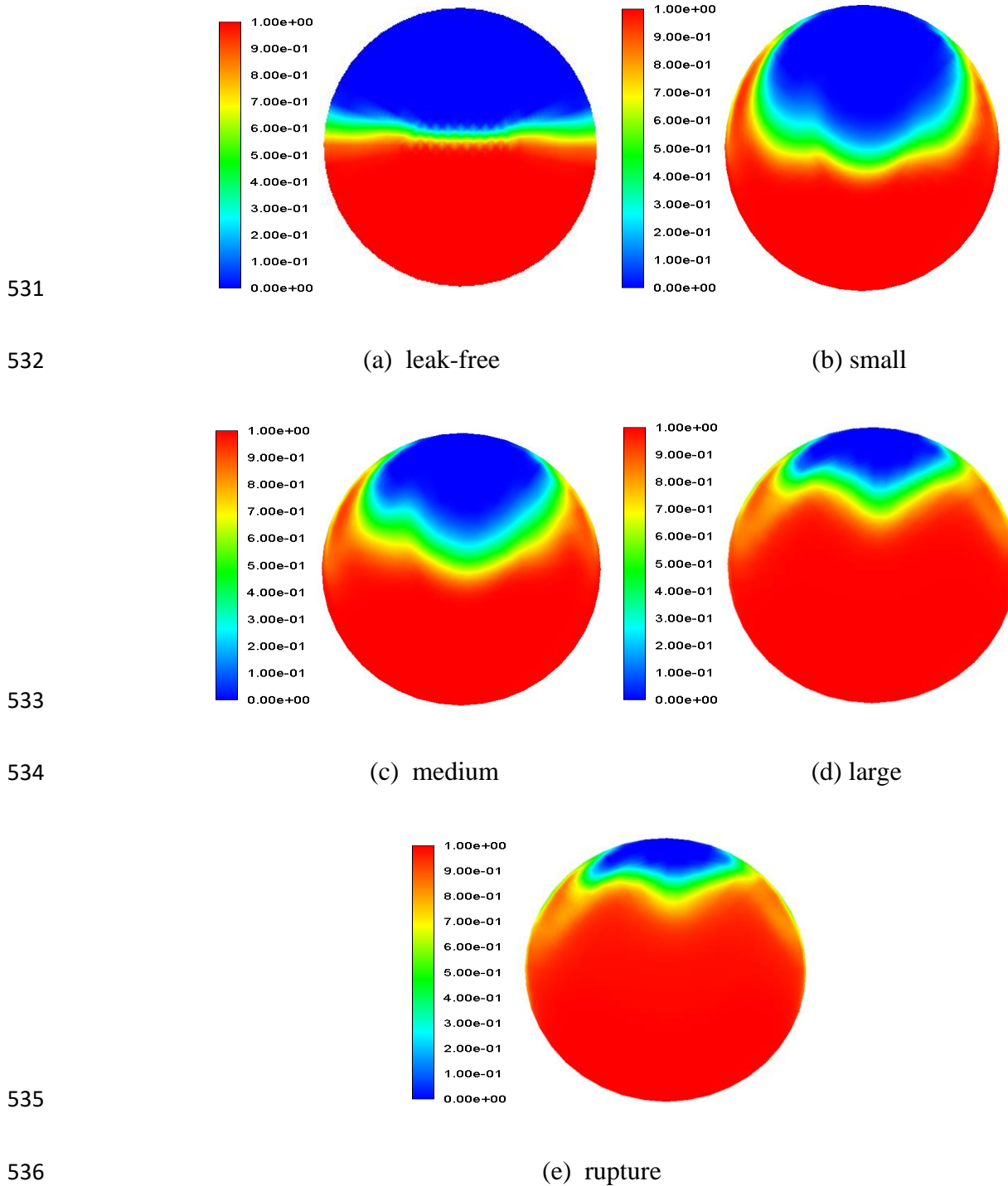
526

(a)

(b)

527

528 **Fig. 8.** Leak sizes variation simulations response; (a) pressure distributions, (b) flow rate. Note  
 529 that the flow rate represents the total flow rate for the two-phases. Note that leak is located at  
 530  $x/2$ , where  $x$  is the pipe length.



537 **Fig. 9.** Liquid volume fraction contour plots at 2.5 m for different leak opening sizes (Red and  
538 blue colours indicate water and air, respectively)

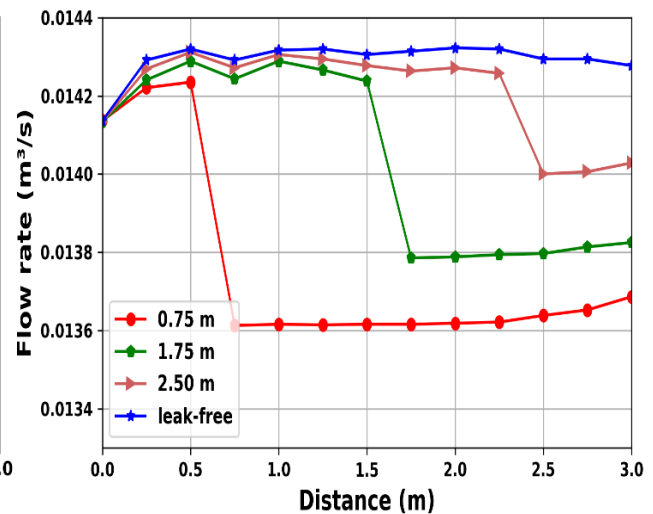
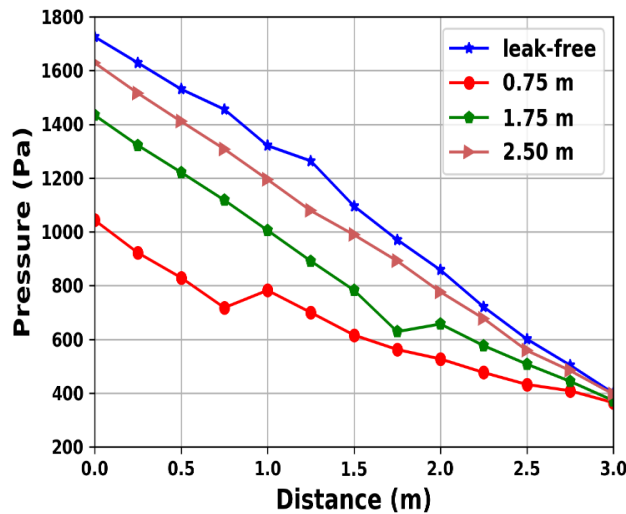
### 539 *5.2 Effect of longitudinal leak location*

540 Various challenges may be experienced in the process of identifying the position of leakage  
541 along a pipe, especially if the pipeline is installed underground or in a subsea environment.  
542 Therefore, it is important to investigate the effect of leak on different locations along the pipe  
543 length for enhancing leak assessment and emergency planning. In this study, the effect of leak on  
544 different longitudinal locations is investigated and analysed. The leak location 1, location 2 and  
545 location 3 are set at 0.75 m, 1.75 m and 2.5 m, respectively away from the pipe upstream. Fig. 10  
546 presents the effect of longitudinal leak detection on the medium pipeline opening size for the  
547 pressure and flow rate responses. Fig. 10(a) shows the effect of different longitudinal leak  
548 locations on the pressure profile. As seen in Fig. 10(a), the occurrence of leakage toward the  
549 downstream of the pipe (at 2.5 m) has little effect on the pressure gradient. However, as the leak  
550 is positioned more towards the upstream section of the pipe, the leak effect become pronounced.  
551 Similar responses have also been observed in the analytical solution in multiphase pipeline  
552 leakage reported by Kam (2010).

553 As it can be observed in Fig. 10(b), the occurrence of leak leads to the flow rate decrement  
554 starting from the leak position downward to pipeline outlet. The leak occurred at 2.50 m away  
555 from the upstream pipeline cause about  $0.00024 \text{ m}^3/\text{s}$  flow rate reduction. By positioning a leak  
556 further upstream of the pipeline, the effect of a leak becomes more pronounced. This agrees with  
557 the analytical solution reported in Kam (2010). If a leak occurs closer to the pipeline upstream, it  
558 is more favourable to detect the leak using the inlet pressure monitoring. The result of the liquid

559 holdup is illustrated in Fig. 10(c). As it is clearly shown, the loss of pressure as the leak location  
 560 closer to the upstream of the pipe reveals increases in liquid holdup accordingly. Fig. 10(d)  
 561 shows a comparison of published liquid holdup (Figueiredo *et al.* 2017) against the result in Fig.  
 562 10(c). the figure reveals a correlation in relative jump, particularly as the leak closer to the  
 563 pipeline downstream.

564 The volume fraction contour plots at 2.75 m for the longitudinal locations are illustrated in Fig.  
 565 11. By comparison, a significant difference can be found in volume fraction as the location of  
 566 leakage changes from the pipe upstream to the outlet. In the absence of leakage, the fraction of  
 567 each phase distributes equally. However, the variation in leak position results in liquid  
 568 accumulation increasing as the leak location changes toward the upstream of the pipeline.

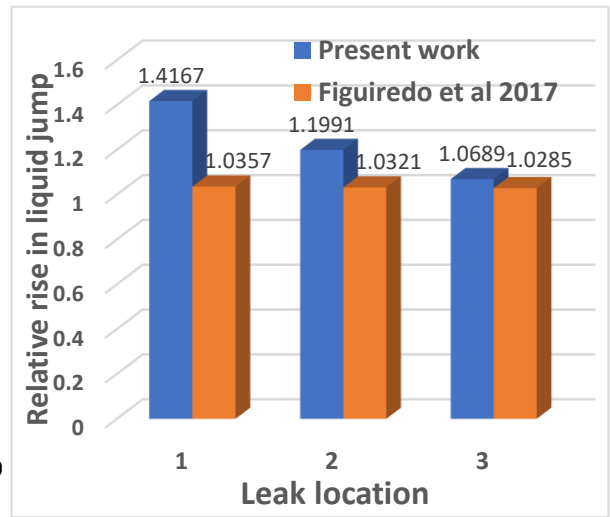
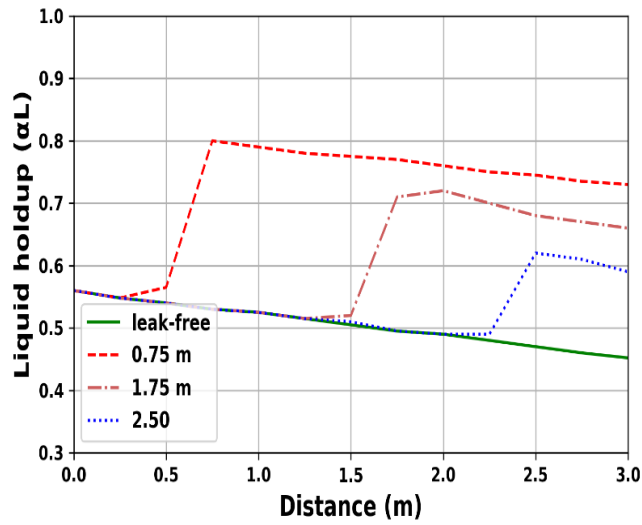


569

(a)

(b)

570



571

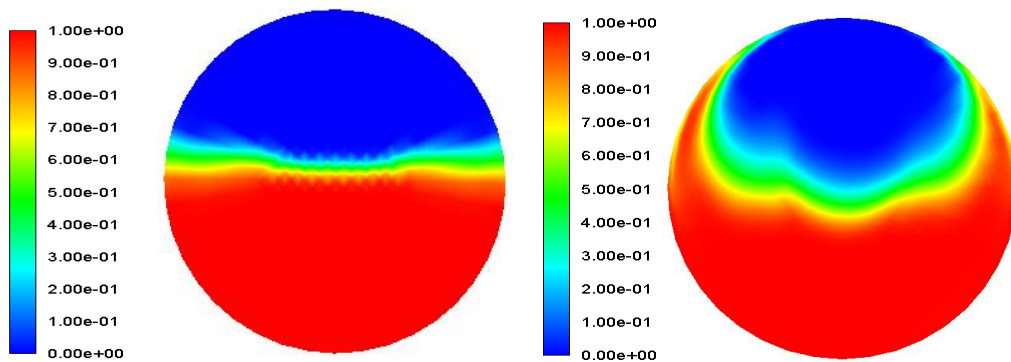
572

(c)

(d)

573 **Fig. 10.** Effect of longitudinal leak locations; (a) pressure distributions, (b) flow rate, (c) liquid  
 574 holdup, (d) liquid holdup comparison with published data. The legend shows different locations  
 575 of leakage from pipe upstream to the downstream. Note that the flow rate represents the total  
 576 flow rate for the two-phases.

577

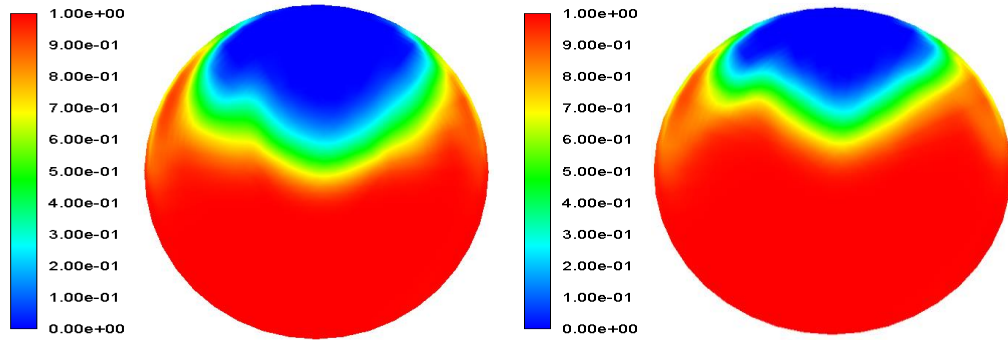


578

(a) leak-free

(b) 2.50 m

579



580

581

(a) 1.75 m

(b) 0.75 m

582

**Fig. 11.** Volume fraction contour plots at 2.75 m for different longitudinal leak locations. (Red

583

and blue colours indicate water and air, respectively).

584

### 585 *5.3 Effect of axial leak positions*

586

In the previous section, the leak was set to locate in the gas phase. Knowledge about pipeline

587

leak position, namely gas-phase, liquid-phase or interface of the two phases is important for

588

enhancing the understanding of leak effect on a multiphase pipeline system. The leak scenarios

589

for the medium and large sizes are considered to study hydraulic behaviours induced by leak at

590

different fluid phases. The leak is located at the middle of the pipe, as shown in Fig. 1. The

591

legend indicates the fluid phases where the leak occurred. The flow parameters that are

592

investigated include the pressure gradient, the total flow rate and the volume fraction of the

593

fluids within the pipeline. The flow parameters variation for the medium leak size under different

594

leak positions is presented in Fig. 12(a). The legend indicates the fluid phases where the leak

595

occurred. As seen in these figures, it is apparent that the location of leakage on the multiphase

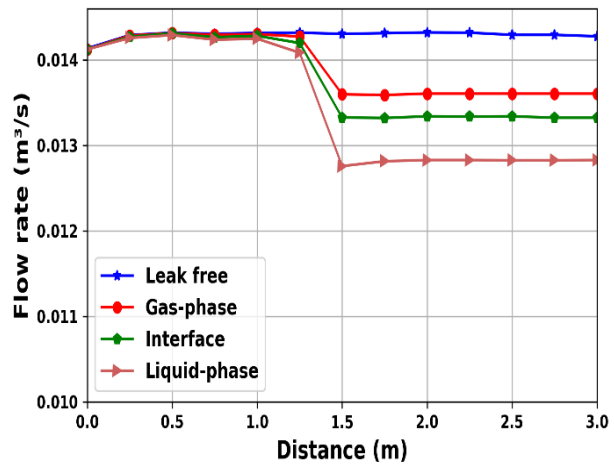
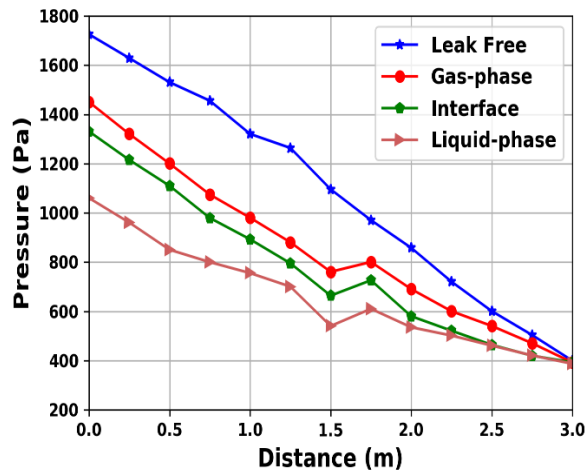
596

pipeline affects the flow pressure profile in the pipeline. A significant effect exists when the leak

597 is situated on the liquid-phase side. Similarly, the flow rate responses in Fig. 1(a) imply that the  
598 maximum total flow rate drop occurs at the liquid-phase axis, while the least drop is observed at  
599 the gas-phase position. Similar behaviour for the case of large leak can also be observed in Fig.  
600 12(b).

601 By comparison, we can find that the influence of pipeline leakage is more pronounced on the  
602 liquid phase than gas or gas-liquid interface, and the reasons are two-fold. Firstly, the leak at the  
603 bottom of the pipeline (liquid-phase) favours the quantity of the pipeline's fluid discharge.  
604 Secondly, the fluids' physical properties could also be another reason for the higher pressure drop  
605 in the liquid phase. For instance, the high density of the liquid may be one of the factors  
606 contributing to the higher pressure drop when the leak is situated in the liquid phase. The gas-  
607 liquid volume fraction distribution for the leak at the gas-phase, liquid-phase and interface of the  
608 two phases are examined using contour plots at 2.5 m away from the pipe upstream. Fig.13  
609 shows the responses of fluids fraction for the same leak scenarios as in Fig. 12(b). The absence  
610 of leak shows that the void fraction and liquid holdup is nearly uniform with the clear interface  
611 between the liquid and gas phase as previously observed in Fig. 12(a) and (b) for the pressure  
612 profile and flow rate responses, respectively. However, Fig. 13(b) shows that the occurrence of a  
613 leak at the gas phase attracts liquid moving from the bottom of the pipeline toward the leak  
614 region. Fig. 13(c) and (d) present the fluids saturation for the leak event at the gas-liquid  
615 interface and liquid phase. The occurrence of a leak at the gas-liquid interface allows air to  
616 diffuse into the water as both phases discharge simultaneously from the pipeline.

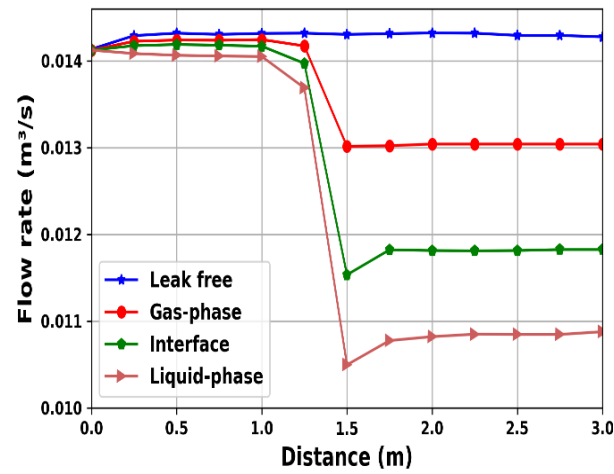
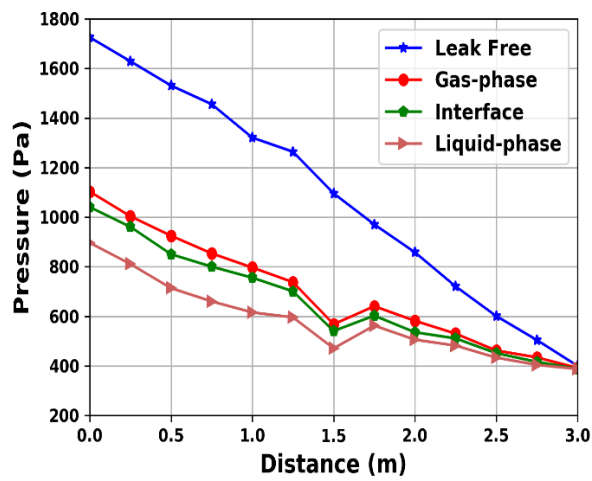
617



618

619

(a)



620

621

(b)

622 **Fig. 12.** Effect of axial leak positions; (a) medium size, (b) large size. (Pressure distributions

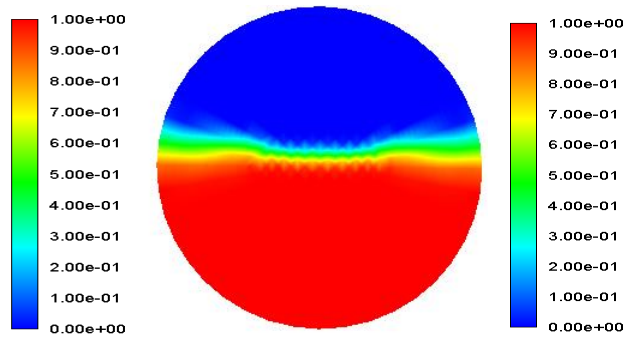
623 (left) and flow rate (right)). Note that the flow rate represents the total flow rate for the two-

624

phases.

625

626

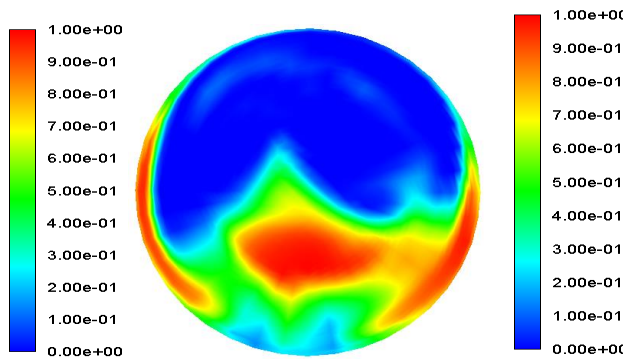


627

(a) leak-free

(b) gas-phase

628



629

(a) interface

(b) liquid-phase

630

**Fig. 13.** Volume fraction contour plots at 2.5 m for leak at different axial positions. (Red and

631

blue colours indicate water and air, respectively. The leak is located at the middle of the

632

pipeline).

633

#### ***5.4 Effect of multiple leakages***

634

The emergence of double leaks on a single pipeline can easily affect the accuracy of detecting

635

pipeline leakage. Therefore, the investigation of multiphase flow in pipe with multiple leaks

636

plays a crucial role in determining the size of the leaks and identify the location of pipeline

637

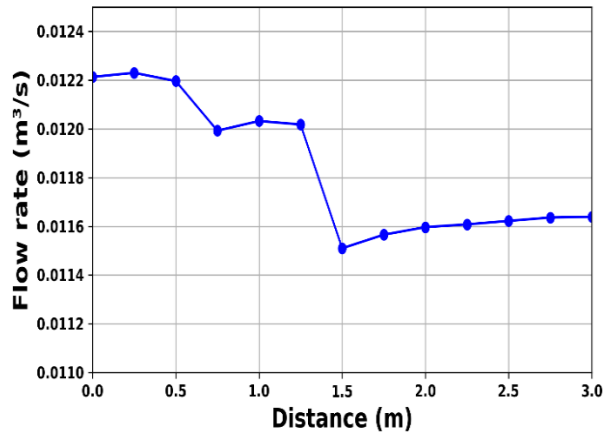
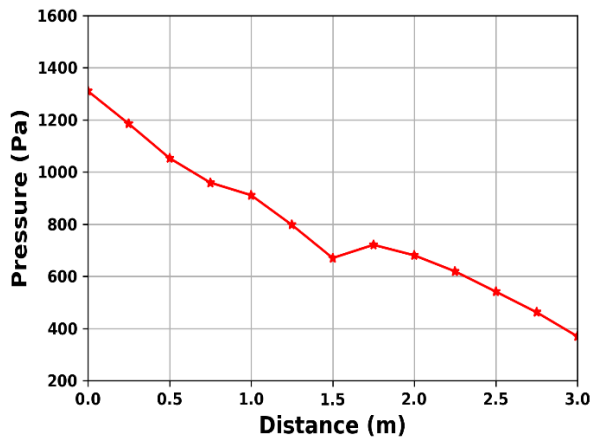
leakage accurately. The impact of double leaks on pipeline leak detection and localisation has

638

been considered and analysed in this study. Fig. 14 illustrate the pressure gradients and the flow

639 rates in various multiple leak scenarios. The first leak location is set at 0.75 m away from the  
640 pipe upstream, while the second leak is located at the 1.5 m, which is the mid-point of the  
641 pipeline. The two leak sizes are chosen among small, medium and large. In all scenarios, the  
642 second hole is chosen to have a medium size. Fig. 14(a), shows the double leak scenario where  
643 the first leak has a small size. The flow responses behave significantly differently with different  
644 leak sizes. The pressure drop for the medium leak size is more significant than that of small size.  
645 It is observed that a small leak position at 0.75 m is difficult to locate if the pressure profile is  
646 employed as an indicator for detecting or locate leak position.

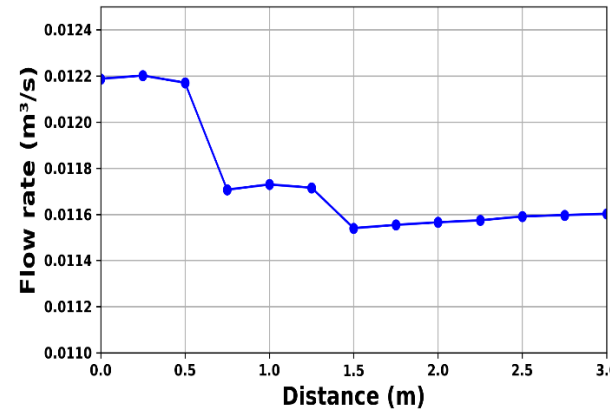
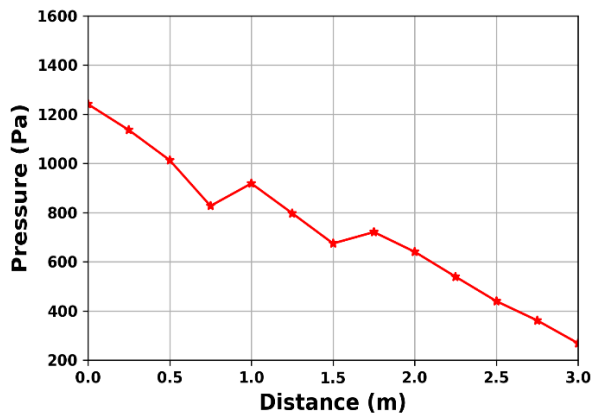
647 Fig. 14(b) illustrates low-medium leak scenarios with equal (medium-medium) leak sizes. The  
648 system responses show that the emergence of the second leak does not cause significant effects  
649 on the pressure drop compared to leak closer to the upstream of the pipeline. A leak closer to the  
650 pipe upstream always results in higher drop in pressure and flow rate than the second leak.  
651 Similar responses are also observed in Fig. 14(c) for the leak scenario with the large-medium  
652 leak located at 0.75 m and 1.5 m away from the upstream of the pipe, respectively. There are two  
653 major observations from the double leak scenarios: Firstly, when there are two leaks with  
654 different leak sizes, the large leak easily masks out the small one. This is because more fluid  
655 tends to escape through the large opening size. Therefore, it causes an increase in pressure drop  
656 around the large leak region. Secondly, in the event of double leaks with equal size, a leak closer  
657 to the pipe upstream has a dominant effect on the flow. This could be linked to higher pressure in  
658 the upstream section of the pipe, leading to more significant loss on the leak closer to the  
659 upstream of the pipe.



660

661

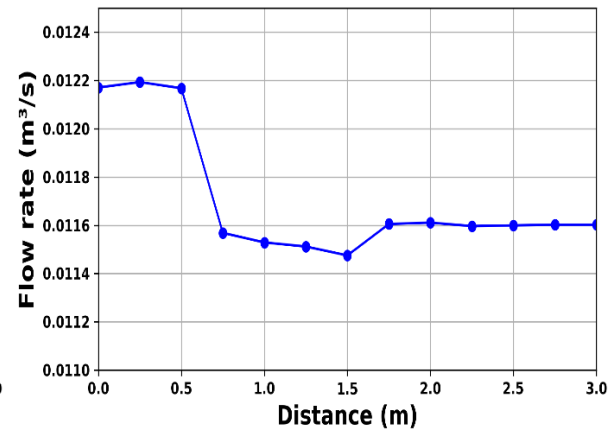
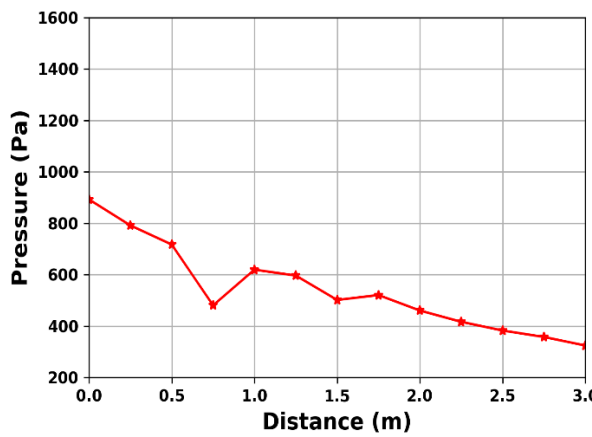
(a) low - medium sizes



662

663

(b) medium - medium sizes



664

665

(c) large - medium sizes

666 **Fig. 14.** Effect of double leaks with different leak sizes. Pressure distributions (left) and flow rate  
667 (right)).

668

## 669 **6. Summary and conclusions**

670 This paper presents a comprehensive simulation and assessment of multiphase flow behaviours  
671 induced by leaks in a subsea pipeline. A 3D CFD model was established to simulate different  
672 scenarios in which leak(s) may occur in subsea pipeline conveying more than one phase at a  
673 time. The VOF model and SST  $k-\omega$  turbulence modelling scheme were applied to simulate the  
674 gas-liquid stratified flow in a horizontal subsea pipeline with a diameter of 60 mm. The  
675 superficial inlet velocities were chosen such that the stratified flow regime was formed. The  
676 simulation results were validated by comparing CFD results with simulation and experimental  
677 data found in the literature. The effect of leak sizes, longitudinal leak locations, multiple  
678 leakages and axial leak positions were analysed in terms of pressure gradient, flow rate and  
679 volume fractions of the gas and liquid phases. The simulation results showed that numerical  
680 simulation could help compile a set of guidelines for conducting prior leak assessment and  
681 contingency planning of accidental leakage of subsea pipeline.

682 It was found that when a pipeline leakage occurs, the fluids flow parameters experienced a  
683 fluctuation, particularly within the vicinity of the leak regions, which makes it possible to detect  
684 and locate the leak position. Leak size has a significant impact on the amount of fluids  
685 discharged through the leak region, which increases with the leak size. The flow parameters  
686 investigated as possible leak detection and localisation indicators are pressure drop, flow rate and  
687 volume fractions. In all cases studied, it was observed that the outlet flow rate is better for leak  
688 detection if the flow transducer is considered as an indicator for pipeline leak detection.  
689 However, upstream pressure is preferred if the pressure transducer is used as a pipeline leak  
690 detection sensor. The volume fractions are believed to be effective for quantifying the leak sizes

691 in the multiphase flow system. Overall, the detection of pipeline leakage appears to be easier if  
692 the pipe opening size is large and located closer to the pipe upstream. However, the impact of the  
693 leak on flow parameters is less significant when the size of the leak is small and closer to the  
694 pipeline outlet. The influence of multiple leakages on a single pipeline is investigated in different  
695 with different hole sizes, which show that effect of the leak in the region closer to the inlet of the  
696 pipeline is more significant than the second leak. Conversely, when double leaks with different  
697 sizes occur, a leak with large size is more detectable than the other.

698 The emphasis of this paper is to investigate the impact of leaks on two-phase gas-liquid flow  
699 behaviours and its consequences in different leak scenarios to improve the understanding of the  
700 leak effect on a multiphase subsea pipeline. The modelling and assessment presented in this  
701 study can be useful for risk assessment and improve the emergency management level.  
702 Therefore, reduce the rate of failure through early detection and localisation of pipeline leakage.  
703 The scope of this study is limited to the modelling of pipeline leakage using a CFD-based  
704 approach. Nevertheless, some areas can be further investigated in future, such as incorporating  
705 effects of temperature, gas compressibility, inlet gas volume fraction, inlet pressure and flow  
706 rate. The potential synergy of Internet of Things (IoT), digital twins and artificial intelligence  
707 (AI) technology which is expected to achieve real-time and dynamic monitoring as assessment,  
708 early notification and decision making for subsea pipeline leak detection, can be explored in the  
709 future.

## 710 **Acknowledgement**

711 The authors acknowledge the support of the Petroleum Technology Development Fund (PTDF),  
712 Abuja Nigeria, for providing funding to MAA under its Overseas Scholarship scheme.

714 **Appendix A. Nomenclature**

$A$	Interface area density
ANOVA	Analysis of Variance
$B$	Damping factor
CFD	Computational Fluid Dynamics
CSF	Continuum Surface Force
$\vec{F}$	Surface tension force
$\vec{g}$	Gravity acceleration force, $m/s^2$
HRIC	High-resolution interface capturing
IOGP	International Association of Oil and Gas Producers
$I$	Unit tensor
$k$	Turbulence kinetic energy, $m^2/s^2$
MAD	Mean Absolute Deviation
$p$	pressure
RANS	Reynolds-Averaged Navier-Stokes
SST	Shear Stress Transport Model
$S_{ij}$	average strain rate
$S_\omega$	source term
$t$	time, $s$
VOF	Volume of Fluid
$\vec{v}$	velocity vector, $m/s$
$\vec{v}^T$	Transpose of the velocity vector, $m/s$
$\omega$	Specific dissipation rate, $1/s$
$x$	Pipe length
1-D	One-dimensional
3-D	Three-dimensional

## Greek symbols

$\rho$	density of fluid
$\nabla$	Gradient operator
$\bar{\tau}$	molecular stress tensor
$\bar{\tau}_t$	turbulent stress tensor
$\mu$	viscosity
$\mu_t$	dynamics viscosity
$\alpha_1$	volume fractions of the secondary phase
$\alpha_2$	volume fractions of the secondary phase
$\beta$	turbulence model constant
$D_\omega^+$	dimensionless specific dissipation rate
$\alpha$	Alpha

716

717 **References**

- 718 Adegboye, M.A., Fung, W.-K., Karnik, A., 2019. Recent advances in pipeline monitoring and  
719 oil leakage detection technologies: principles and approaches. *Sensors*, 19(11), 2548.  
720 <https://doi.org/10.3390/s19112548>.
- 721 Ajao, L., Adedokun, E., Nwishieyi, C., Adegboye, M., Agajo, J., Kolo, J., 2018. An anti-theft oil  
722 pipeline vandalism detection: embedded system development. *Intern. J. of Eng. Sci. and*  
723 *Applica.* 2(2), 55-64. <https://dergipark.org.tr/en/pub/ijesa/38052/408770>.
- 724 Akhlaghi, M., Mohammadi, V., Nouri, N. M., Taherkhani, M., Karimi, M., 2019. Multi-Fluid  
725 VoF model assessment to simulate the horizontal air–water intermittent flow. *Chem. Eng.*  
726 *Res. and Design*, 152, 48-59. <https://doi.org/10.1016/j.cherd.2019.09.031>.
- 727 Alghurabi, A., Mohyaldinn, M., Jufar, S., Younis, O., Abduljabbar, A., Azuwan, M., 2021. CFD  
728 numerical simulation of standalone sand screen erosion due to gas-sand flow. *J. of Nat. Gas*  
729 *Sci. and Eng.* 85, 1-15. <https://doi.org/10.1016/j.jngse.2020.103706>.
- 730 Ali, I.T., 2017. CFD prediction of stratified and intermittent gas-liquid two-phase turbulent pipe  
731 flow using RANS models, PhD thesis, Faculty of Science and Engineering. The University of  
732 Manchester, United Kingdom.
- 733 Ali, J.M., Hoang, N.H., Hussain, M.A., Dochainc, D., 2015. Review and classification of recent  
734 observers applied in chemical process systems. *Com. & Chem. Eng.* 76, 27-41.  
735 <https://doi.org/10.1016/j.compchemeng.2015.01.019>.
- 736 ANSYS, 2017. *Ansys Fluent 18.1 Users Guide*. ANSYS, Canonsburg, PA.

737 Araújo, M.V., Neto, S.R., Lima, A.G. B., 2013. Theoretical evaluation of two-phase flow in a  
738 horizontal duct with leaks. *Adv. in Chem. Eng. and Sci.* 3, 6-14.  
739 <http://dx.doi.org/10.4236/aces.2013.34A1002>.

740 Araújo, M.V., Neto, S.R., Lima, A.G.B., de Luna, F.D.T., 2014. Hydrodynamic study of oil  
741 leakage in pipeline via CFD. *Adv. in Mech. Eng.* 6, 170178.  
742 <https://doi.org/10.1155/2014/170178>.

743 Behari, N., Sheriff, M. Z., Rahman, M. A., Nounou, M., Hassan, I., Nounou, H., 2020. Chronic  
744 leak detection for single and multiphase flow: A critical review on onshore and offshore  
745 subsea and arctic conditions. *J. of Nat. Gas Sci. and Eng.*, 103460.  
746 <https://doi.org/10.1016/j.jngse.2020.103460>.

747 Ben-Mansour, R., Habib, M.A., Khalifa, A., Youcef-Toumi, K., Chatzigeorgiou, D., 2012.  
748 Computational fluid dynamic simulation of small leaks in water pipelines for direct leak  
749 pressure transduction. *Computer & Fluids.* 57, 110-123.  
750 <https://doi.org/10.1016/j.compfluid.2011.12.016>.

751 bin Md Akib, A., bin Saad, N. Asirvadam, V., 2011. Pressure point analysis for early detection  
752 system. In *IEEE 7th International Colloquium on Signal Processing and its Applications*,  
753 Penang, Malaysia, 4-6 March 2011. DOI: 10.1109/CSPA.2011.5759852.

754 Brackbill, J. U., Kothe, D. B., Zemach, C., 1992. A continuum method for modeling surface  
755 tension. *J. of Comp. Phy.* 100, 335-354. [https://doi.org/10.1016/0021-9991\(92\)90240-Y](https://doi.org/10.1016/0021-9991(92)90240-Y).

756 Chen, L., Jin, P., Yang, J., Li, Y., Song, Y., 2021. Robust Kalman filter-based dynamic state  
757 estimation of natural gas pipeline networks. *Math. Prob. in Eng.* 2021, 1-10.  
758 <https://doi.org/10.1155/2021/5590572>.

759 Chen, Q., Shen, G., Jiang, J.C., Diao, X., Wang, Z. Ni, L., Dou, Z., 2018. Effect of rubber  
760 washers on leak location for assembled pressurised liquid pipeline based on negative pressure  
761 wave method. *Pro. Safety and Env. Prot.* 119, 181-190.  
762 <https://doi.org/10.1016/j.psep.2018.07.023>.

763 Chinello, G., Ayati, A.A., McGlinchey, D., Ooms, G., Henkes, R., 2019. Comparison of  
764 computational fluid dynamics simulations and experiments for stratified air-water flows in  
765 Pipes. *J. of Fluids Eng.* 141(5), 051302. <https://doi.org/10.1115/1.4041667>.

766 Cramer, R., Shaw, D., Tulalian, R., Angelo, P., van Stuijvenberg, M., 2015. Detecting and  
767 correcting pipeline leaks before they become a big problem. *Marine Tech. Soc. J.* 49(1), 31-  
768 46. <https://doi.org/10.4031/MTSJ.49.1.1>.

769 Datta, S., Sarkar, S., 2016. A review on different pipeline fault detection methods. *J. of Loss*  
770 *Prev. in the Proc. Indus.*, 41, 97-106. <https://doi.org/10.1016/j.jlp.2016.03.010>.

771 Dasgupta, S., 2016. Shell spill 88,200 gallons of oil into Gulf of Mexico.  
772 <https://news.mongabay.com/2016/05/shell-spills-90000-gallons-crude-oil-gulf-mexico/>  
773 (accessed 20 June 2019).

774 De Sousa, C.A., Romero, O.J., 2017. Influence of oil leakage in the pressure and flow rate  
775 behaviors in pipeline. *Latin American J. of Energy Res.* 4(1), 17-29.  
776 <https://doi.org/10.21712/lajer.2017.v4.n1.p17-29>.

777 Elaoud, S., Hadj-Taïeb, L. Hadj-Taïeb, E., 2010. Leak detection of hydrogen–natural gas  
778 mixtures in pipes using the characteristics method of specified time intervals. *J. of Loss*  
779 *Preve. in the Proc. Indus.* 23(5), 637-645. <https://doi.org/10.1016/j.jlp.2010.06.015>.

780 Espedal, M., 1998. An experimental investigation of stratified two-phase pipe flow at small  
781 inclinations. PhD thesis, in: Department of Applied Mechanics, Thermo-and Fluid Dynamics.  
782 Norwegian University of Science and Technology (NTNU), Norway.

783 Fu, H., Yang, L., Liang, H., Wang, S., Ling, K., 2020. Diagnosis of the single leakage in the  
784 fluid pipeline through experimental study and CFD simulation. *Journal of Petroleum Science  
785 and Engineering*, 193, 107437. <https://doi.org/10.1016/j.petrol.2020.107437>.

786 Figueiredo, A.B., Sondermann, C.N., Patricio, R.A., Bodstein, G.C., Rachid, F.B., 2017. A leak  
787 localization model for gas-liquid two-phase flows in nearly horizontal pipelines. Paper  
788 presented at the ASME International Mechanical Engineering Congress and Exposition, (pp.  
789 1-10), Tampa, Florida, USA. <https://doi.org/10.1115/IMECE2017-71512>.

790 Guerriero, M., Wheeler, F., Koste, G., Dekate, S., Choudhury, N., 2016. Bayesian data fusion for  
791 pipeline leak detection. Paper presented at the 2016 19th International Conference on  
792 Information Fusion (FUSION). Heidelberg, Germany, July 5-8 2016.

793 Ijaola, A. O., Farayibi, P. K., Asmatulu, E., 2020. Superhydrophobic coatings for steel pipeline  
794 protection in oil and gas industries: a comprehensive review. *J. of Nat. Gas Sci. and Eng.*  
795 83(2020) 103544. <https://doi.org/10.1016/j.jngse.2020.103544>.

796 Joling, D., 2017. Alaska underwater pipeline leak may have started in December; 2017.  
797 <https://apnews.com/81cc24dd5195459497f1be530d5bdb56> (access 21 March 2019).

798 Kam, S.I., 2010. Mechanistic modeling of pipeline leak detection at fixed inlet rate. *J. of Petrol.  
799 Sci. and Eng.* 70(4), 145-156. <https://doi.org/10.1016/j.petrol.2009.09.008>.

800 Kanin, E. A., Osiptsov, A. A., Vainshtein, A. L., Burnaev, E. V., 2019. A predictive model for  
801 steady-state multiphase pipe flow: Machine learning on lab data. *J. of Petrol. Sci. and Eng.*  
802 180(2019), 727-746. <https://doi.org/10.1016/j.petrol.2019.05.055>.

803 Karim, M.Z.A., Alrasheedy, A., Gaafar, A., 2015. Compensated mass balance method for oil  
804 pipeline leakage detection using SCADA. *Int. J. Comput. Sci. Secur. (IJCSS)*, 9, 293-302.

805 Kazeem, B. A., Yskandar, H., Bolanle, T. A., Adnan, M. A., 2017. Towards achieving a reliable  
806 leakage detection and localisation algorithm for application in water piping networks: An  
807 overview. *IEEE Access*, 5, 20272-20285. DOI: 10.1109/ACCESS.2017.2752802.

808 Lazhar, A., Hadj-Taïeb, L., Hadj-Taïeb, E., 2013. Two leaks detection in viscoelastic pipeline  
809 systems by means of transient. *J. of Loss Prevent. in the Pro. Industr.* 26(6), 1341-1351.  
810 <https://doi.org/10.1016/j.jlp.2013.08.007>.

811 Li, X., Chen, G., Zheng, R., Zhu, H., Fu, J., 2018. Simulation and assessment of underwater gas  
812 release and dispersion from subsea gas pipelines leak. *Pro. Safety and Env. Protec.* 119, 46-  
813 57. <https://doi.org/10.1016/j.psep.2018.07.015>.

814 Li, X., Chen, G., Khan, F., Xu, C., 2019a. Dynamic risk assessment of subsea pipelines leak  
815 using precursor data. *Ocean Engineering.* 178, 156-169.  
816 <https://doi.org/10.1016/j.oceaneng.2019.02.009>.

817 Li, X., Chen, G., Zhu, H., 2017. Modelling and assessment of accidental oil release from  
818 damaged subsea pipelines. *Marine pollution bulletin*, 123(1-2), 133-141.  
819 <https://doi.org/10.1016/j.marpolbul.2017.09.004>.

820 Li, X., Chen, G., Zhang, R., Zhu, H., Xu, C., 2019b. Simulation and assessment of gas dispersion  
821 above sea from a subsea release: A CFD-based approach. *Intern. J. of Naval Arch. and Ocean*  
822 *Eng.* 11(1), 353-363. <https://doi.org/10.1016/j.ijnaoe.2018.07.002>.

823 Liu, C., Li, Y., Xu, M., 2019. An integrated detection and location model for leakages in liquid  
824 pipelines. *J. of Petrol. Sci. and Eng.* 175, 852-867.  
825 <https://doi.org/10.1016/j.petrol.2018.12.078>.

826 Lo, S., Tomasello, A., 2010. Recent progress in CFD modelling of multiphase flow in horizontal  
827 and near-horizontal pipes. In 7th North American Conference on Multiphase Technology.  
828 BHR Group, Banff, Canada, June 02, 2010.

829 Mohammed, A. I., Oyeneyin, B., Atchison, B., Njuguna, J., 2019. Casing structural integrity and  
830 failure modes in a range of well types-a review. *J. of Nat. Gas Sci. and Eng.* 68(2019),  
831 102898. <https://doi.org/10.1016/j.jngse.2019.05.011>.

832 Molina-Espinosa, L., Cazarez-Candia, O. Verde-Rodarte, C., 2013. Modeling of incompressible  
833 flow in short pipes with leaks. *J. of Petrol. Sci. and Eng.* 109, 38-44.  
834 <https://doi.org/10.1016/j.petrol.2013.08.007>.

835 Movley, C., 2005. Pipeline corrosion from induced AC. In *Corrosion 2005*, Houston, Texas,  
836 April 2005. OnePetro.

837 Bolotina, I., Borikov, V., Ivanova, V., Mertins, K., Uchaikin, S., 2018. Application of phased  
838 antenna arrays for pipeline leak detection. *J. of Petrol. Sci. and Eng.*, 161, 497-505.  
839 <https://doi.org/10.1016/j.petrol.2017.10.059>.

840 Muggleton, J. M., Hunt, R., Rustighi, E., Lees, G., Pearce, A., 2020. Gas pipeline leak noise  
841 measurements using optical fibre distributed acoustic sensing. *J. of Nat. Gas Sci. and Eng.*  
842 78, 1-12. <https://doi.org/10.1016/j.jngse.2020.103293>.

843 Ranawat, N. S., Nandwana, B. P., 2021. Study of the effect of leak location in water pipeline  
844 using CFD. In *Recent Advances in Mechanical Engineering* (pp. 173-181). Springer,  
845 Singapore. [https://doi.org/10.1007/978-981-15-8704-7\\_21](https://doi.org/10.1007/978-981-15-8704-7_21).

846 Saeedipour, M., Vincent, S., Pirker, S., 2019. Large eddy simulation of turbulent interfacial  
847 flows using Approximate Deconvolution Model. *International J. of Mul. Flow*, 1(112), 286-  
848 299. <https://doi.org/10.1016/j.ijmultiphaseflow.2018.10.011>.

849 Scott, R. P., 2018. Should we call the neighbors? Voluntary deliberation and citizen complaints  
850 about oil and gas drilling. *Energy Policy*. 115, 258-272.  
851 <https://doi.org/10.1016/j.enpol.2018.01.017>.

852 Scott, R. P., Scott, T. A., 2019. Investing in collaboration for safety: Assessing grants to states  
853 for oil and gas distribution pipeline safety program enhancement. *Energy Policy*, 124, 332-  
854 345. <https://doi.org/10.1016/j.enpol.2018.10.007>.

855 Singh, J.P., Kumar, S., Mohapatra, S., 2017. Modelling of two phase solid-liquid flow in  
856 horizontal pipe using computational fluid dynamics technique. *Intern. J. of Hyd. Energy*,  
857 42(31), 20133-20137. <https://doi.org/10.1016/j.ijhydene.2017.06.060>.

858 Strand, O., 1993. An experimental investigation of stratified two-phase flow in horizontal pipes,  
859 PhD thesis, University of Oslo, Oslo, Norway.

860 Sun, Y., Cao, X. Liang, F., 2019. Investigation on underwater spreading characteristics and  
861 migration law of oil leakage from damaged submarine pipelines. *Pro. Safety. and Env. Pro.*  
862 127, 329-347. <https://doi.org/10.1016/j.psep.2019.05.030>.

863 Syed, M. M., Lemma, T. A., Vandrangi, S. K., Ofei, T. N., 2020. Recent developments in model-  
864 based Fault detection and diagnostics of gas pipelines under transient conditions. *J. of Nat.*  
865 *Gas Sci. and Eng.* 83, 1-21. <https://doi.org/10.1016/j.jngse.2020.103550>.

866 Wang, X., Ghidaoui, M. S., 2018. Pipeline leak detection using the matched-field processing  
867 method. *J. of Hydraulic Eng.* 144(6), 04018030. [https://doi.org/10.1061/\(ASCE\)HY.1943-7900.0001476](https://doi.org/10.1061/(ASCE)HY.1943-7900.0001476).

868

869 Wang, X., Tan, Y., Zhang, T., Xiao, R., Yu, K., Zhang, J., 2021. Numerical study on the  
870 diffusion process of pinhole leakage of natural gas from underground pipelines to the soil. *J.*  
871 *of Nat. Gas Sci. and Eng.* 87, 1-14. <https://doi.org/10.1016/j.jngse.2020.103792>.

872 Wei, O.Y., Masuri, S.U., 2019. Computational fluid dynamics analysis on single leak and double  
873 leaks subsea pipeline leakage. *CFD Letters*, 11, 95-107.

874 Yang, Z., Fan, S., Xiong, T., 2010. July. Simulation and numerical calculation on pipeline  
875 leakage process. *IEEE 2nd International Symposium on Information Engineering and*  
876 *Electronic Commerce*, Ternopil, Ukraine, July 23-25 2010. DOI:  
877 10.1109/IEEC.2010.5533189.

878 Zhu, H., Lin, P., Pan, Q., 2014. A CFD (computational fluid dynamic) simulation for oil leakage  
879 from damaged submarine pipeline. *Energy*, 64, 887-899.  
880 <https://doi.org/10.1016/j.energy.2013.10.037>.